LBL-15469 c.2

Lawrence Berkeley Laboratory
UNIVERSITY OF CALIFORNIA

Physics, Computer Science & Mathematics Division

RECEIVED
LAWRENCE
BERKELEY LABORATORY

FEB 28 1983

LIBRARY AND
DOCUMENTS SECTION

Presented at the SLAC Summer School, Stanford Linear Accelerator Center, Stanford, CA, August 16-27, 1982; and to be published in the Proceedings

EXPECTATIONS FOR OLD AND NEW PHYSICS AT HIGH ENERGY COLLIDERS

R.N. Cahn

December 1982

Prepared for the U.S. Department of Energy under Contract DE-AC03-76SF00098

LBL-15469 c.2

DISCLAIMER

This document was prepared as an account of work sponsored by the United States Government. While this document is believed to contain correct information, neither the United States Government nor any agency thereof, nor the Regents of the University of California, nor any of their employees, makes any warranty, express or implied, or assumes any legal responsibility for the accuracy, completeness, or usefulness of any information, apparatus, product, or process disclosed, or represents that its use would not infringe privately owned rights. Reference herein to any specific commercial product, process, or service by its trade name, trademark, manufacturer, or otherwise, does not necessarily constitute or imply its endorsement, recommendation, or favoring by the United States Government or any agency thereof, or the Regents of the University of California. The views and opinions of authors expressed herein do not necessarily state or reflect those of the United States Government or any agency thereof or the Regents of the University of California.

December 1982 LBL-15469

Expectations for Old and New Physics at High Energy Colliders

R. N. Cahn

CERN, Geneva
and
Lawrence Berkeley Laboratory,
University of California, Berkeley CA 94720[*]

[*] Permanent address.

PREFACE

During the past year, the first data from the SPS collider at CERN have become available. The initial results are only a glimpse at a new energy regime and we can reasonably expect an increase in the extent of the data by a factor of 10^4 to 10^5. Moreover, within a few years, the Fermilab Tevatron Collider will be in operation with a center of mass energy nearly four times as great as that at CERN. Beyond these machines are other possibilities: a high luminosity pp machine at Brookhaven with a center of mass energy of 0.8 TeV; a $p\bar{p}$ or pp machine in the LEP tunnel at CERN; a "desetron" in the southwestern United States with many TeV in the center of mass. The purpose of these lectures is to provide an orientation for the wealth of data that these machines will provide.

It is quite impossible to cover comprehensively the topic of high energy hadronic collisions in two lectures or ten. As a first step in reducing the scope of the subject I have omitted any discussion of multiparticle production at low momentum transfer. Since these events make up the bulk of the cross section, this is a serious omission indeed. Nevertheless, the remaining topics are so extensive that a complete review of them would probably require the entirety of the Summer School rather than the two lectures I have available.

To reduce the task even further I have relied on a particular advantage I bring to the assignment: I am not an expert on the topic of hadronic interactions. In deciding what material to include in the lectures, I simply asked myself what I would like to know about the subject, with the hope that this would correspond to the wishes of most of the participants in the Summer School. In this way I decided to restrict myself to two topics: very soft physics and very hard physics. The first lecture, then, is devoted to total cross sections, the ratio of the real to the imaginary

part of the forward scattering amplitude, and the slope parameter. The second discusses, at the most elementary level, lepton pair production, Z^0 production, high transverse momentum, and heavy flavor production.

The first topic is so old that it has almost become new. Many younger physicists are unaware of the very beautiful work on analyticity, which once played such a central role in the concerns of high energy physics. Indeed, many who were once familiar with this topic may enjoy refreshing their memories. Moreover, the colliders are taking us a long way toward the elusive asymptopia where most of the rigorous theorems apply.

The second topic is by comparison new, but runs the risk of becoming worn out, so much has been said of high transverse momentum and the like. The intent here is to use the most direct means available for estimating the cross sections of interest while eschewing all considerations of theoretical refinements such as higher order corrections in QCD. This is dictated both by lack of space and time and by my lack of expertise; it is justified by the inherent uncertainties in the best of calculations.

How interesting are $p\bar{p}$ colliders? Aren't the Z^0 factories about to be built at SLAC and CERN much more interesting? My own bias is that if nothing unexpected happens, the results from the Z^0 factories will be cleaner and thus more susceptible to interpretation. But if nothing unexpected happens, we shall not have learned very much. We should hope for the unanticipated which may give us the new clues we need. In these lectures I show what we should expect, in the hope that it will provide a standard against which we can measure to find discrepancies that will lead to a better understanding.

These are truly lectures, not reviews. Consequently, I have not tried to give complete references to the original literature, but instead

have often chosen to cite reviews that I found useful. I apologize to the many authors whose contributions have thus been slighted.

I would like to thank CERN and the A. P. Sloan Foundation which provided support during the time the lectures were initially written. Also, I would like to thank Jacques Prentki for the hospitality of the Theory Group at CERN. Thanks are also due to Maurice Jacob and Andre Martin for their interest and assistance. Most especially, thanks are due to Marty Block with whom most of the material in the first lecture was prepared jointly. This work was also supported in part by the Director. Office of Energy Research, Office of High Energy and Nuclear Physics, Division of High Energy Physics of the U.S. Department of Energy under Contract DE-AC03-76SF00098.

I. Elastic Scattering

1.1 Geometrical Picture

We begin our study of elastic scattering at very high energies by recollecting some basic concepts from ordinary scattering theory [Schiff, 1968;Eden, 1967;Jackson, 1973]. We neglect spin even though we are interested primarily in pp and $p\bar{p}$ scattering. The intent here is to develop a geometrical picture of the scattering which will provide a suggestive language and some intuition for the subject.

The standard partial wave expansion for the scattering amplitude is

$$f(\theta,k)=\frac{1}{k}\sum_l(2l+1)P_l(\cos\theta)a_l(k), \tag{1}$$

where

$$a_l(k)=\frac{\exp(2i\delta_l)-1}{2i}, \tag{2}$$

and δ_l is the phase shift in the lth partial wave. At very high energies, elastic scattering involves very many partial waves so it is convenient to convert the sum over l into an integral. Let k be the center of mass momentum, θ the center of mass scattering angle, and q the momentum transfer. Then $q^2=4k^2(\sin\theta/2)^2$. A classical description of the scattering would introduce the impact parameter, b, which is related to the angular momentum by

$$bk=l+\frac{1}{2} \tag{3}$$

The extra 1/2 is thrown in for convenience and in recognition of its appearance in the WKB approximation.

To convert Eq.(1) to an integral, we replace $\sum_l\to\int dl\to\int k\,db$ and $a_l(k)\to a(b,k)$. We need also to express $P_l(\cos\theta)$ in terms of b and q.

For large l, we have [Erdélyi,1953]

$$P_l(\cos\theta)\to J_0((2l+1)\sin\theta/2) \tag{4}$$

With these replacements, Eq.(1) becomes

$$f(\theta,k)=2k\int_0^\infty bdbJ_0(qb)a(b,k) \tag{5}$$

or, using the integral representation of J_0 [Abramowitz and Stegun, 1964, p. 360]

$$J_0(z)=\frac{1}{2\pi}\int_0^{2\pi}d\phi\exp(iz\cos\phi) \tag{6}$$

it is simply

$$f(\theta,k)=\frac{k}{\pi}\int d^2b\,\exp(i\mathbf{q}\cdot\mathbf{b})a(b,k) \tag{7}$$

With the standard non-relativistic normalization, we have

$$\sigma_{el}=\int d\Omega|f|^2=\int d^2q\frac{|f|^2}{k^2}=4\int d^2b|a(b,k)|^2, \tag{8}$$

and

$$\sigma_{tot}=\frac{4\pi}{k}Im\,f(0,k)=4\int d^2b\,Im\,a(b,k). \tag{9}$$

where the latter follows from the optical theorem [Schiff, 1968]. The amplitude in impact parameter space, $a(b,k)$ is still of the form of Eq. (2). Thus it lies in the usual Argand plot shown in Fig. 1a. Elastic scattering corresponds to δ being real. If there is inelastic scattering as well, then δ has a positive imaginary part and $a(b,k)$ lies inside the Argand circle.

Total absorption corresponds to $Im\,\delta=\infty$ or $a(b,k)=i/2$. Thus a black disc of radius R gives a total cross section (see Eq.(9)) $2\pi R^2$ and an elastic cross section of πR^2 (see Eq.(8)).

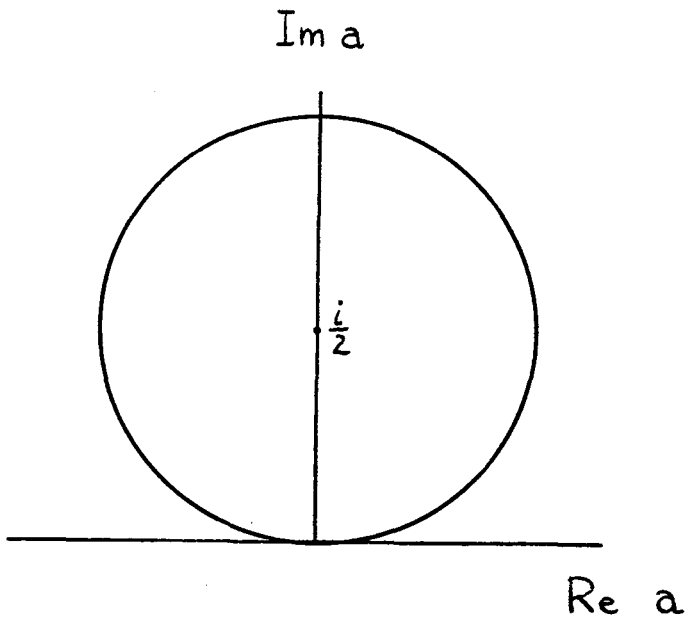

Fig. 1.a. The Argand circle inside which the partial wave amplitude, $a_l(k)$, Eq. (2), must lie.

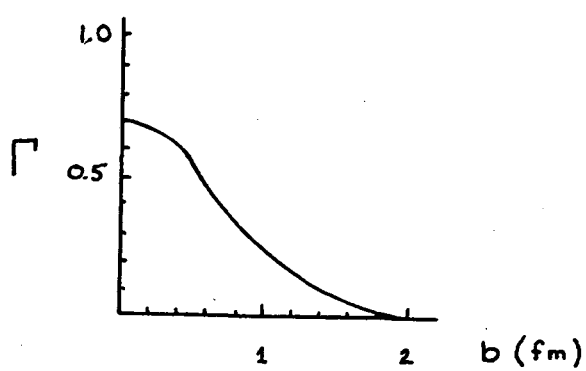

Fig. 1.b. The profile of the proton, $\Gamma = |\frac{2}{i}a(b,k)|$ vs. b , for a purely imaginary Gaussian elastic amplitude. See Eq. (13).

We can translate the scattering amplitude into an amplitude in impact parameter space by inverting the Fourier transform in Eq.(7). Thus we find

$$a(b,k) = \frac{1}{4\pi k}\int d^2q \exp(-i\mathbf{q}\cdot\mathbf{b}) f(\theta,k) \tag{10}$$

Let us apply this simple geometrical picture to elastic pp scattering using the parameters appropriate to ISR data. The amplitude will be taken to be purely imaginary (the ratio of the real to the imaginary part is less than 0.1 at these energies) with a dependence on q^2 of the form $\exp(-Bq^2/2)$. The value measured for B at the ISR is around 13 GeV^{-2} [Giacomelli and Jacob, 1979]. Using the optical theorem, Eq.(9), we find the amplitude

$$f = \frac{ik\sigma_{tot}}{4\pi}\exp(-Bq^2/2) \tag{11}$$

and the elastic cross section

$$\sigma_{el} = \int d\Omega |f|^2 = \int |f|^2 \frac{\pi dq^2}{k^2} = \frac{\sigma_{tot}^2}{16\pi B} \tag{12}$$

Moreover, we can calculate the profile of the proton in impact parameter space.

$$a(b,k) = \frac{i\sigma_{tot}}{16\pi^2}\int d^2q \exp(-Bq^2/2)\exp(-i\mathbf{b}\cdot\mathbf{q})$$

$$= \frac{i\sigma_{tot}}{16\pi}\frac{2}{B}\exp(-b^2/2B) \tag{13a}$$

$$= \frac{2i\sigma_{el}}{\sigma_{tot}}\exp(-b^2/2B) \tag{13b}$$

At zero impact parameter, $a(0,k) = i\sigma_{tot}/(8\pi B) = i\,43\,\mathrm{mb}\,(8\cdot\pi\cdot 13\mathrm{GeV}^{-2})^{-1}\cdot(0.389\,\mathrm{mb\,GeV}^2)^{-1} = 0.34\,i$. This is 68% black. As the impact parameter increases, the proton becomes progressively more transparent. See Fig.lb.

1.2 Analyticity

Having begun with a very physical approach to the scattering of high energy particles, we reverse our direction completely to consider the most abstract techniques, those based on analyticity [Eden, 1967; Martin and Cheung, 1970; Jackson, 1973]. Analytic properties of the scattering amplitude seemed a central aspect of hadronic physics before the advent of QCD [Chew, 1966]. While dynamical calculations based on QCD seem more compelling than approaches based on analyticity, there remains a truly impressive edifice built by Gell-Mann, Goldberger, Lehmann, Martin, Mandelstam, and others which is part of the cultural heritage of particle physics. Here we shall treat the topic in a brutally simplistic way, striving only to reveal results of direct applicability to high energy scattering.

The forward scattering amplitude for pp scattering is a function of s, the square of the center of mass energy.[1] It is the boundary value of an analytic function. By this we mean that there is an analytic function of s, say $F(s)$, such that if we let s be just above the real axis, say $x + i\epsilon$, then $F(x + i\epsilon)$ is the scattering amplitude for center of mass energy squared x. The function $F(s)$ is analytic in the s-plane, except for cuts (and poles) along the real axis. See Fig. 2a. One cut begins at $4m_p^2$ and extends to infinity along the positive real axis. There is also a left hand cut. Below the left hand cut, $F(s)$ represents the scattering amplitude of $p\bar{p}$ scattering. If the value of s is $-x - i\epsilon$, $F(s)$ represents the scattering amplitude for $p\bar{p}$ scattering at a center of mass energy squared of $x + 4m_p^2$. When s is just below the left hand cut, it corresponds to the value of u for the $p\bar{p}$ scattering. It is often useful to use a variable $\nu = (s - u)/4m_p$ which has nicer symmetry than u or s, but at high energies and fixed t we can just as well use s itself.

Fig. 2.a. The complex s-plane with left and right hand cuts. The pp elastic amplitude is evaluated just above the right hand cut and the $p\bar{p}$ elastic amplitude is evaluated just below the left hand cut.

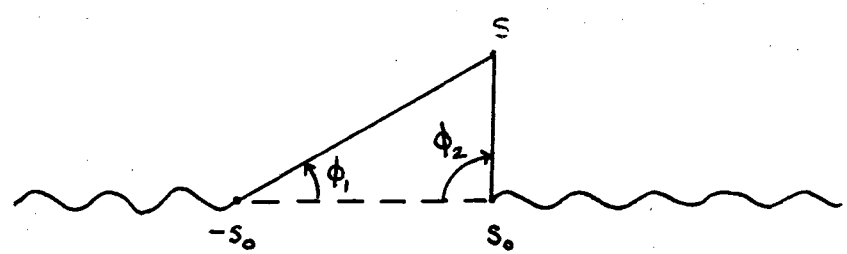

Fig. 2.b. The cut complex s-plane for the function g_+ of Eq.(16). The value of the function is

$$g_+(s) = |s_0 + s|^\alpha e^{i\alpha\phi_1} + |s_0 - s|^\alpha e^{-i\alpha\phi_2}.$$

We shall consider the Lorentz invariant amplitude $\mathcal{M}$,which for convenience we normalize so that the optical theorem reads

$$\sigma = -Im\mathcal{M}/s \tag{14}$$

where we have ignored m_p^2 relative to s.[2] It is very useful to define two amplitudes which are combinations of the pp and p$\overline{\text{p}}$ elastic amplitudes:

$$\mathcal{M}_{\pm} = \frac{1}{2}(\mathcal{M}_{p\overline{p}} \pm \mathcal{M}_{pp}). \tag{15}$$

The amplitude $\mathcal{M}_+$ is even under $s \to -s$, while $\mathcal{M}_-$ is odd (again, we really should be using the variable ν). As a prototypical example, consider the function

$$g_+(s) = (s_0 - s)^\alpha + (s_0 + s)^\alpha, \tag{16}$$

This function has branch points at $\pm s_0$. We can take the branch cuts to extend from s_0 to infinity and from $-s_0$ to negative infinity along the real axis. We define the function so that it is real along the real axis between $-s_0$ and s_0. See Fig.2b.

Just above the right hand cut, for $s \gg s_0$,

$$g_+(s) \approx |s|^\alpha(1 + \exp(-i\pi\alpha)) = 2\cos(\pi\alpha/2)|s|^\alpha \exp(-i\pi\alpha/2), \tag{17}$$

while just below the left hand cut

$$g_+(s) \approx |s|^\alpha(\exp(-i\pi\alpha) + 1) = 2\cos(\pi\alpha/2)|s|^\alpha \exp(-i\pi\alpha/2), \tag{18}$$

This function is even and real analytic (that is, it is real on the real axis). Moreover, (since it is real analytic) its value just above the cut is just the complex conjugate of its value just below the cut, as one easily verifies. It has all the properties we want for the forward scattering amplitude. Its imaginary part would be related to the cross section. Just below threshold, it is purely real. From this example, we infer that even amplitudes which behave asymptotically as s^α have the phase $\exp(-i\pi\alpha/2)$. This inference can be made rigorous with the Phragmèn-Lindelöf theorem [Titchmarsh, 1939]. The corresponding analysis for odd amplitudes shows that their phase is $\exp(i\pi(1-\alpha)/2)$ if their power behavior is s^α.

Of course, not all amplitudes need have power law behavior. An example of an even function of a different sort is

$$\tilde{g}_+(s) = \frac{1}{2}[\ln((s_1 + s)/s_0) + \ln((s_1 - s)/s_0)], \tag{19}$$

which has the same sort of cut structure as before and which we can define so that it is real on the real axis between the two branch points. We then find that above the right hand cut (and below the left hand cut), for $s \gg s_0$

$$\tilde{g}_+(s) \approx \ln(s/s_0) - \frac{i\pi}{2}. \tag{20}$$

1.3 The Froissart Bound

Before the operation of the ISR , it appeared that all hadron-hadron total cross sections might become constant at high energies (this

was believed inspite of the apparent rise in the K^+p cross section). It was known on fundamental grounds that the cross sections could not grow faster than $\ln^2 s$ - the Froissart bound [Froissart, 1961]- but this limit seemed quite irrelevant. Now the pp cross section appears to be growing as $\ln^2 s$, though that may not continue.

We present here a derivation of the Froissart bound based on two fundamental results which we take as given [Martin and Cheung, 1970]:

i. The scattering amplitude $\mathcal{M} \sim \sqrt{s} f$ grows no faster than s^2.

ii. For fixed s (i.e. k^2), the amplitude is analytic in the region $|q|^2 < 4m_\pi^2$.

We use (2) and evaluate $\mathcal{M}$ at $q = 2im_\pi$ using Eq.(7).

$$\begin{aligned} \mathcal{M} &\sim s \int d^2b \exp(i\mathbf{q}\cdot\mathbf{b})\, a(b,s) \\ &\sim s \int bdb\, d\phi\ \exp(-2m_\pi b\cos\phi)\, a(b,s) \\ &\sim s \int bdb \exp(2m_\pi b)\, a(b,s) \qquad < Cs^2. \end{aligned} \tag{21}$$

The third line is a rough approximation valid for $m_\pi b \gg 1$.

We seek to maximize the cross section, subject to this constraint. Clearly it is best to make $a(b,s)$ purely imaginary. Also, it is best to keep all the contributions at the lowest possible value of b in order to minimize the above integral. Thus we take $a(b,s) = i$ for $b < b_c$ and $a(b,s) = 0$ for $b > b_c$. A rough evaluation of the integral gives us a limit for b:

$$\exp(2m_\pi b_c) \approx Cs,$$

$$b_c \approx \frac{1}{2m_\pi} \ln(s/s_0), \tag{22}$$

where s_0 is an unknown scale.

Now using Eq.(9), we find

$$\begin{aligned} \sigma_{tot} &= 4\int d^2b\, Im\, a(b,s) = 4\pi b_c^2 \\ &= \frac{\pi}{m_\pi^2}(\ln(s/s_0))^2 \qquad \approx 60\text{mb}\cdot(\ln(s/s_0))^2. \end{aligned} \tag{23}$$

Of course, all the hard work has been done for us by our friends like Martin who proved (i) and (ii).

1.4 Pomeranchuk Theorems

When the highest energy data available came from Serpukhov, it seemed that the pp total cross section was becoming constant. In such circumstances, the Pomeranchuk theorem would apply [Pomeranchuk, 1958]. This theorem states that if pp and $p\bar{p}$ (or more generally, ab and $a\bar{b}$) cross sections become constant asymptotically and if the ratio of the real to the imaginary part of the forward scattering amplitude increases less rapidly than $\ln s$, the two cross sections become equal asymptotically.

It is easy to understand this result by considering examples. If pp and $p\bar{p}$ cross sections become constant, then $\mathcal{M}_+ \sim -is$. If $\mathcal{M}_-$ grows slower than this, then surely the difference cross section falls with s. Suppose then that $\mathcal{M}_-$ grows as $s(\ln(s/s_0) - i\pi/2)^\beta$. If $\beta = 1$ the difference cross section is asymptotically a non-zero constant, but the ratio of the real to the imaginary part grows as $\ln s$. If $\beta < 1$,the real part

over the imaginary part grows as $(\ln s)^{\beta}$, that is, less rapidly than $\ln s$, but then the cross section difference goes as $(\ln s)^{\beta-1}$, that is, it falls to zero. Certainly β cannot be greater than one. Thus, we see that the Pomeranchuk theorem holds for amplitudes of this class.

This lovely theorem is of no use if the cross sections rise. There are useful theorems, however, that speak to this situation. Suppose the pp and $p\bar{p}$ cross sections grow as $(\ln s)^{\gamma}$. Then we can show that the difference of the cross sections cannot grow faster than $(\ln s)^{(\gamma/2)}$ [Eden, 1966; Kinoshita, 1966].

The proof goes as follows. Referring to Fig.1a, we see that since the amplitude $a(b)$ must lie in the Argand circle (we drop the indication of the energy at which the amplitude is evaluated),

$$|Re\, a(b)|^2 \leq Im\, a(b).$$

In the previous section, we showed that the impact parameters that contribute significantly to scattering must lie within some value b_c which grows as $\ln s$. Thus we can approximate the scattering amplitude, Eq. (7) as

$$f(q=0) = \frac{k}{\pi}\int d^2b\, a(b) \approx 2k\int_0^{b_c} bdb\, a(b). \tag{24}$$

It follows that

$$\begin{aligned} |Ref(0)| &\approx 2k\left|\int_0^{b_c} bdb\, Re\, a(b)\right| \\ &\leq 2k\int_0^{b_c} bdb|Re\, a(b)| \\ &\leq 2k\int_0^{b_c} bdb[Im\, a(b)]^{1/2} \end{aligned} \tag{25}$$

Next we apply the Cauchy-Schwartz inequality

$$\begin{aligned} |Ref(0)| &\leq 2k\left[\int_0^{b_c} bdb\, Im\, a(b)\right]^{1/2}\left[\int_0^{b_c} bdb\right]^{1/2} \\ &\leq 2k\left(\frac{\sigma_{tot}}{8\pi}\right)^{1/2}\left(\frac{1}{2}b_c^2\right)^{1/2} \\ &\leq \text{constant}\cdot k\cdot(\ln s/s_0)^{\gamma/2}(\ln s/s_0). \end{aligned} \tag{26}$$

Now the generic form for the odd amplitude is

$$f_- \sim k(\ln s/s_0 - i\pi/2)^{\gamma'}, \tag{27}$$

so

$$\gamma' \leq \gamma/2 + 1. \tag{28}$$

But the difference of the cross sections goes as

$$\Delta\sigma \sim (\ln s/s_0)^{\gamma'-1} \leq \text{constant}(\ln s/s_0)^{\gamma/2}, \tag{29}$$

as we wished to show.

1.5 Testing Analyticity

An analytic function has real and imaginary parts which are intimately linked. The relation may be expressed by Cauchy's equations or by the vanishing of a contour integral around a region free of singularities. Traditionally, analyticity of scattering amplitudes has been tested using dispersion relations, that is to say, using the contour integral. In this way, the real part of the amplitude can be calculated from the imaginary part, which is known from the measured cross section. A behavior must be postulated for the cross section above the energies where it has been measured. Another problem occurs when the amplitude can have an imaginary part in an unphysical region. We shall use a simpler approach that is effective in the high energy domain where the cross section is relatively smooth.

The real part of the forward scattering amplitude is measured by observing the interference between the hadronic and Coulombic scattering. A naive analysis indicates that at small momentum transfer squared, t, the full amplitude is a sum

$$k^{-1} f(s,t) = \frac{i+\rho}{4\pi}\sigma_{tot}\, e^{bt/2} + \frac{2\alpha}{t} \tag{30}$$

where the first term is hadronic and the second Coulombic. See Fig. 3. The ratio of the real to the imaginary part of the hadronic amplitude is indicated by ρ and $\alpha = 1/137$ is the fine structure constant. By fitting this form, the value of ρ can be deduced.

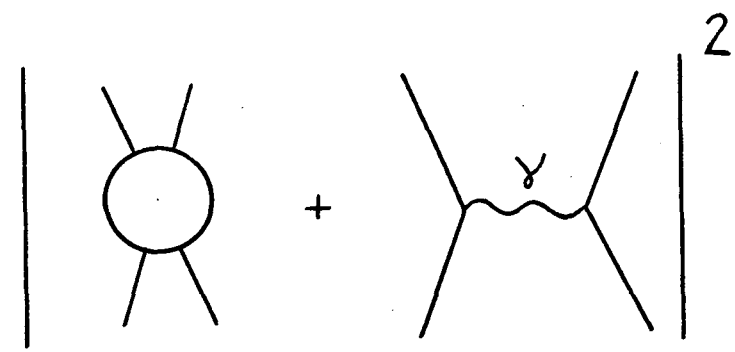

Fig. 3. The elastic pp amplitude as a sum of hadronic and Coulombic interactions. The interference is used to determine the phase of the hadronic amplitude.

In fact, this treatment is not really adequate. The Coulomb amplitude is not precisely as we have written it because there is in addition the mysterious Coulomb phase. In fact, the Coulomb amplitude is not well defined because the scattering wave function contains in the exponential a term $\ln kr$ as well as the standard kr term. This technical complication is well understood and the appropriate corrections established. [Bethe, 1958; West and Yennie, 1968; Cahn, 1982b]

The recent use of the ISR to study $p\bar{p}$ interactions has provided a unique opportunity to measure ρ for this process, with a high intensity, monochromatic beam. Some data collected by the Louvain- Northwestern collaboration are shown in Fig. 4 [Louvain -Northwestern Collaboration, 1982].

Rather than using dispersion relations, we shall test analyticity by fitting the data directly with complex amplitudes with the proper behavior [Eden, 1967; Bourrely and Fischer, 1973]. We parameterize the even amplitude in terms of real constants [Cahn, 1982a; Block and Cahn, 1982a]

$$\mathcal{M}_+ = -is\left[A + \frac{B(\ln s/s_0 - i\pi/2)^2}{1 + a(\ln s/s_0 - i\pi/2)^2}\right] + C, \tag{31}$$

and first consider the case $a = 0$. Then, from Eqs.(30) and (31),

$$\sigma_+ = A + B(\ln^2 s/s_0 - \pi^2/4), \tag{32}$$

which saturates the form of the Froissart bound, and which has often been used in fitting the pp cross section data. Permitting the parameter a to take on small positive values allows for a deviation from this form.

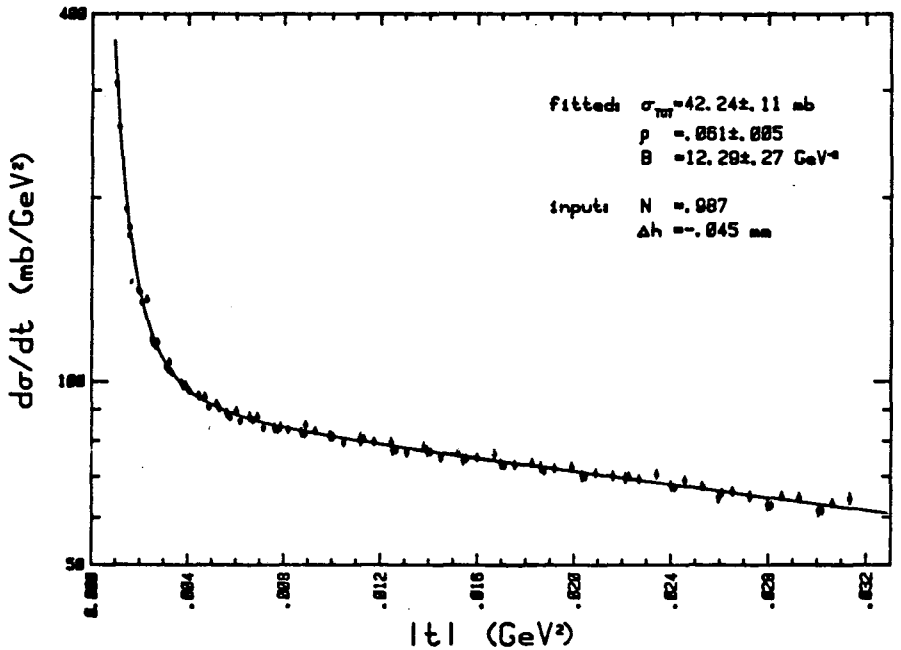

Fig. 4.a. Data on elastic pp scattering at the ISR taken by the Louvain-Northwestern Collaboration, 1982. Below $-t = 0.002\,\mathrm{GeV}^2$ the sharp Coulomb peak is visible. The gentle slope is due to hadronic scattering Between these is the interference region. The data were taken at $\sqrt{s} = 52.8\,\mathrm{GeV}$.

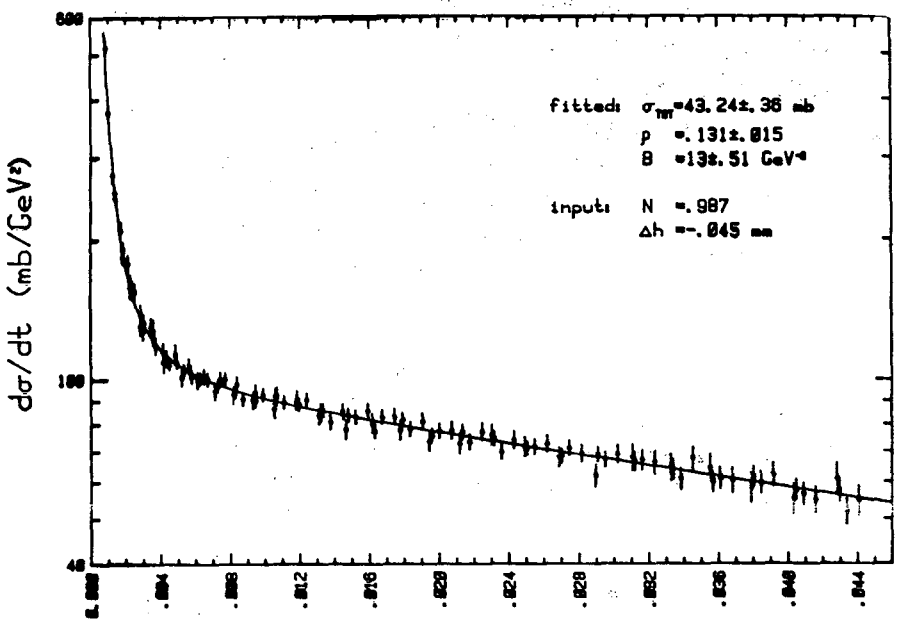

Fig. 4.b. Data for elastic $p\bar{p}$ scattering at the ISR. [Louvain-Northwestern Collaboration, 1982].

Indeed, asymptotically the form gives a <u>constant</u> cross section, $\sigma_+(\infty) = A + B/a$. The constant C is permitted by the requirements of analyticity for the even amplitude and corresponds to a subtraction constant in the usual dispersion relation treatment. We shall show that C is unimportant in the region of interest, as we might expect since it lacks the factor of s present in the dominant terms. We shall also see that very fine fits are obtained with $a = 0$. Thus, just three parameters, A (in mb), B (in mb), and s_0(in GeV^2), are needed to parameterize the even amplitude [3]. The parameter a is useful, however, for it will provide a means of estimating our uncertainty when we try to extrapolate our fit to higher energies.

The odd amplitude is known to be dominated by a piece with the approximate behaviour $s^{1/2}$ (that is, $\sigma_{p\bar{p}} - \sigma_{pp} \sim s^{-1/2}$). We take the power, α and the magnitude, D, of the amplitude as parameters and write

$$\mathcal{M}_- = Ds^{\alpha} \exp[i\pi(1-\alpha)/2]. \tag{33}$$

Later, we shall consider odd amplitudes with unconventional asymptotic behaviour in an attempt to establish limits on the presence of such terms. For the purpose of finding an adequate fit to the present data, they are unnecessary.

The cross sections and ρ values may be obtained directly from Eqs.(31) and (33). If $a = 0$, the resulting forms are especially simple:

$$\sigma_{pp} = A + B(\ln^2 s/s_0 - \pi^2/4) + Ds^{\alpha-1}\cos(\pi\alpha/2),$$
$$\sigma_{p\bar{p}} = A + B(\ln^2 s/s_0 - \pi^2/4) - Ds^{\alpha-1}\cos(\pi\alpha/2),$$
$$\rho_{pp} = \frac{\pi B}{\sigma_{pp}}\ln s/s_0 + \frac{Ds^{\alpha-1}}{\sigma_{pp}}\sin(\pi\alpha/2),$$
$$\rho_{p\bar{p}} = \frac{\pi B}{\sigma_{p\bar{p}}}\ln s/s_0 - \frac{Ds^{\alpha-1}}{\sigma_{p\bar{p}}}\sin(\pi\alpha/2). \tag{34}$$

In Fig. 5, we show the result of fitting Eqs.(31) and (33) to the available data above $s^{1/2} = 5$ GeV. It is clear that the fits are quite successful and there is no apparent violation of analyticity since our fits incorporate analyticity in their very form (at least far from the actual thresholds). In Table I are displayed the values found for the various parameters, together with those for some additional fits to be discussed shortly.

The simplest fit (#1 in Table I) gives an acceptable χ^2/d.f. and provides a reliable means of interpolating the available data for the cross section and ρ values. The second fit allows a non-zero value for a and the best fit is obtained for $a = 0.0050 \pm 0.0031$. We can say that the data do not require $a \neq 0$, but that a small value is permitted. The third fit allows for $C \neq 0$, but the result shows that little is gained by allowing this freedom.

Extrapolating the present fit to collider energies is a speculation, but it is more than just curve fitting because of the constraints imposed by analyticity. However, a bias is introduced by our choice of the $\ln^2 s$ parameterization of the existing data. The present rise in the cross section need not persist indefinitely. The introduction of the parameter $a > 0$ yields a cross section which has a $\ln^2 s$ dependence near the minimum of the cross section but which is asymptotically constant. Of course, that the data slightly prefer a small positive value for a is not necessarily an indication that the cross sections are going to become constant asymptoti-

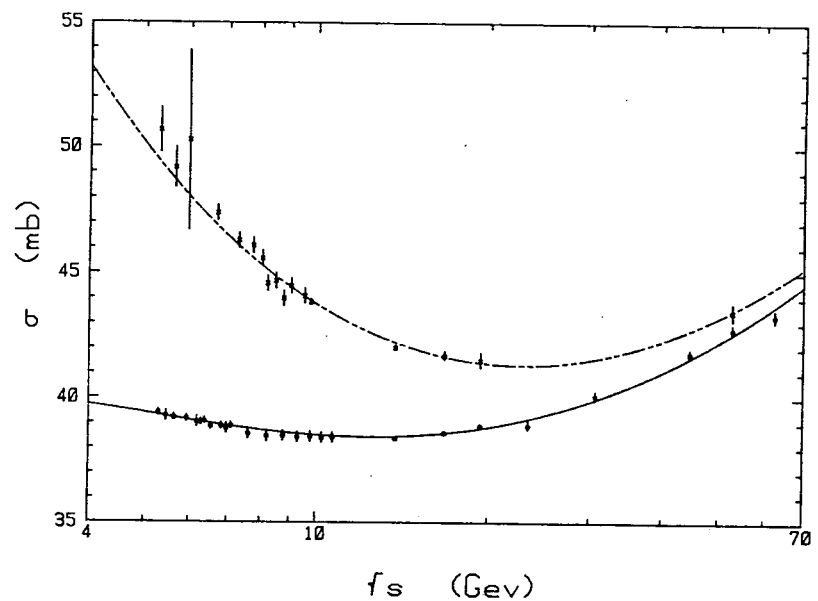

Fig. 5.a. Fit to pp (solid curve) and $p\bar{p}$ (dot-dash) total cross section data using the five parameter fit, #1 of Table I. See Eq. (34) [Block and Cahn, 1982a] .

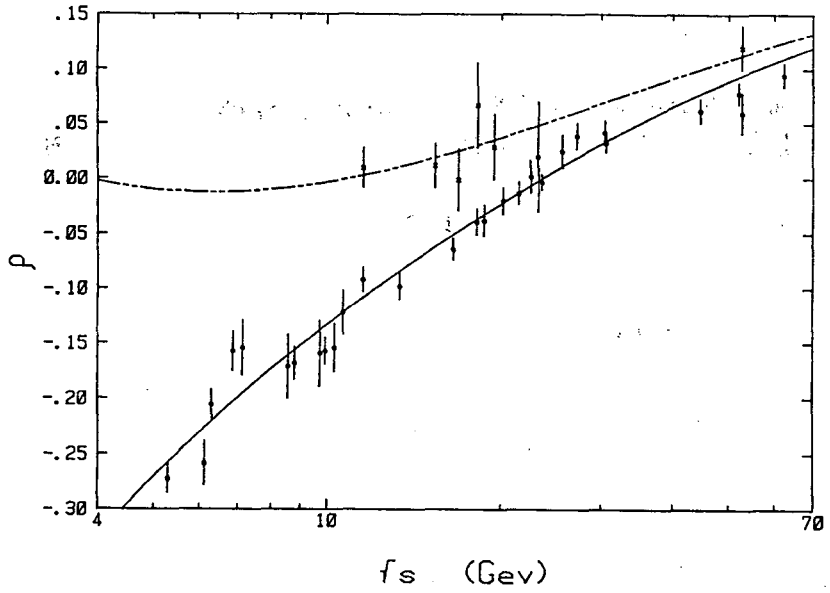

Fig. 5.b. Fit to ρ values for pp (solid curve) and p$\bar{\text{p}}$ (dot-dash) using Fit #1 of Table I. See Eq. (34). [Block and Cahn, 1982a]

Table I. Parameters for the best fits to the cross-section and ρ values for pp and p$\bar{\text{p}}$ data.The even amplitude is given in Eq.(31) . The parameters a and C are set equal to zero except in Fits #2 and #3. The odd amplitude for the first three fits is given by Eq.(33). For the last three fits, the odd amplitude is a sum of this term and one term from among the three Odderons, Eqs.(37a)-(37c). [Block and Cahn, 1982a]

	#1	#2	#3	#4	#5	#6
A(mb)	41.77 $\pm$0.04	41.74 $\pm$0.04	41.77 $\pm$0.04	41.77 $\pm$0.04	41.74 $\pm$0.04	41.70 $\pm$0.05
B(mb)	0.68 $\pm$0.01	0.66 $\pm$0.02	0.68 $\pm$0.01	0.69 $\pm$0.02	0.69 $\pm$0.01	0.66 $\pm$0.01
s_0(GeV^2)	343. $\pm$8.	338. $\pm$8.	344. $\pm$8.	345. $\pm$8.	350. $\pm$8.	356. $\pm$10.
D (mb GeV$^{2-2\alpha}$)	$-$39.0 $\pm$1.7	$-$38.7 $\pm$1.6	$-$39.2 $\pm$1.8	$-$41.7 $\pm$2.4	$-$40.8 $\pm$1.8	$-$35.2 $\pm$2.2
α	0.48 $\pm$0.01	0.49 $\pm$0.01	0.48 $\pm$0.01	0.46 $\pm$0.02	0.49 $\pm$0.01	0.50 $\pm$0.02
a		0.0050 $\pm$0.0031				
C(mb GeV^2)			5.0 $\pm$10.6			
E(mb)				$-$0.26 $\pm$0.13	$-$0.10 $\pm$0.04	$-$0.04 $\pm$0.02
$\chi^2/d.f.$	86.7/73	84.0/72	86.5/72	82.6/72	80.1/72	81.8/72

cally. We consider the difference between the $a = 0$ and $a \neq 0$ fits as providing an estimate of the uncertainty in our extrapolation.

In Fig.6 we show the five parameter fit ($a = 0, C = 0$) and the six parameter fit ($a = 0.0050, C = 0$) extrapolated to collider energies. These fits are simultaneously constrained by data for cross sections and ρ values, for both pp and $p\bar{p}$. In Table II we display some values obtained in these fits, including extrapolations to collider energies. The uncertainties quoted are just those due to the uncertainties for the parameters as determined by the fits. We note that the $a \neq 0$ fit predicts a cross section at $s^{1/2} =$ 540 GeV of 66.0 mb $\pm$ 2.8 mb, while the $a = 0$ fit gives 70.9 mb $\pm$ 0.6 mb. This difference is in rough accord with the result that the best fit for a differs from zero by a little less than two standard deviations: $a = 0.0050 \pm 0.0031$.

Preliminary data from the CERN SPS Collider are now available. The UA-4 Collaboration has reported that it finds, by extrapolating the differential cross section to the $t = 0$ point [UA4 Collaboration, 1982b]

$$(1 + \rho^2)\sigma_{tot} = 66 \pm 7\text{mb}. \tag{35}$$

Referring to Fig. 5, we see that at $s^{1/2} = 540\,\text{GeV}, \rho^2 \approx 0.02 - 0.03$, if the cross section is nearer to 65 mb than to 70 mb. Thus we interpret the UA-4 result as

$$\sigma_{tot} = 64 \pm 7\text{mb} \tag{36}$$

which is in agreement with either the $a = 0$ or $a = 0.0050$ fit. Clearly, higher precision measurements will be of great interest.

Table II. Values of σ and ρ at selected energies. Fit #1 has $a = 0$. Fit #2 has $a = 0.0050$. See Table I for a complete listing of the parameters.[Block and Cahn, 1982a]

	σ_{pp}(mb)	$\sigma_{p\bar{p}}$(mb)	ρ_{pp}	$\rho_{p\bar{p}}$
$\sqrt{s} = 23.5$ GeV				
Fit #1	39.2±0.03	41.3±0.07	0.00±0.001	0.05±0.003
Fit #2	39.2±0.04	41.3±0.07	0.00±0.002	0.05±0.003
$\sqrt{s} = 62.5$ GeV				
Fit #1	43.7±0.1	44.5±0.1	0.11±0.003	0.12±0.002
Fit #2	43.8±0.1	44.6±0.1	0.10±0.005	0.12±0.005
$\sqrt{s} = 540$ GeV				
Fit #1	70.9±0.6	71.0±0.6	0.20±0.002	0.20±0.002
Fit #2	66.0±2.8	66.1±2.8	0.14±0.03	0.14±0.03
$\sqrt{s} = 2000$ GeV				
Fit #1	99.6±1.2	99.6±1.2	0.20±0.001	0.20±0.001
Fit #2	82.3±8.0	82.3±8.0	0.12±0.03	0.12±0.03

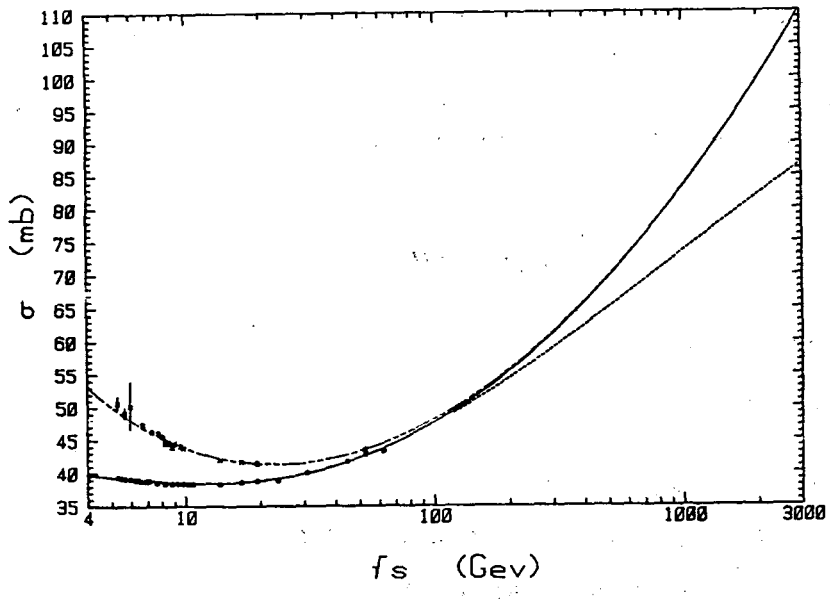

Fig. 6.a. Extrapolations of Fits #1 and #2 of Table I. At high energies, the upper curve is Fit #1 (a=0) and the lower curve is Fit #2 (a=0.0050). At lower energies, the fits are indistinguishable. At high energies, the pp and $p\bar{p}$ cross sections are nearly equal , but at lower energies the $p\bar{p}$ cross section exceeds that of pp. [Block and Cahn, 1982a]

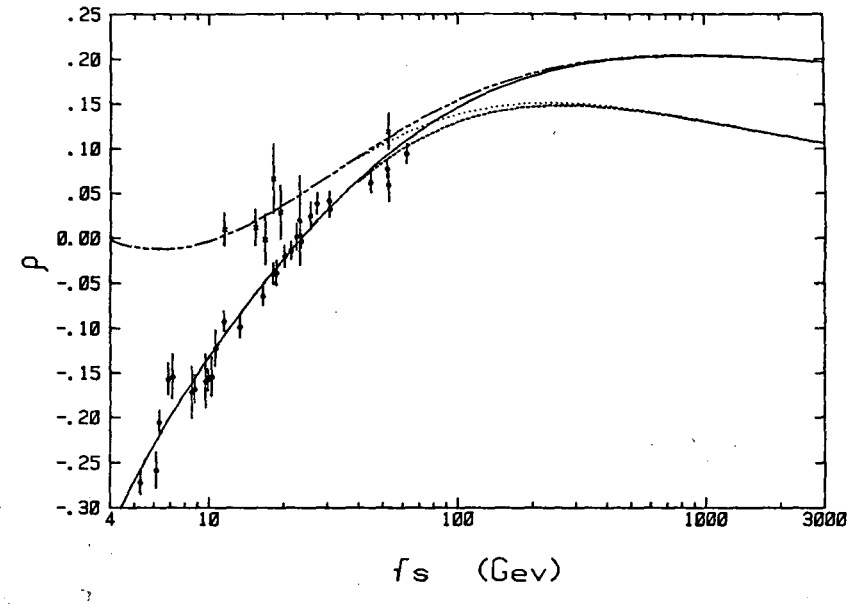

Fig. 6.b. Extrapolations of Fits #1 and #2 for the ρ values. At high energies, the upper curve is Fit #1 and the lower is Fit #2. At low energies, the fits coincide and the upper curve is for $p\bar{p}$. See Table II. [Block and Cahn,1982a]

1.6 The Odd Amplitude

Even before the recent ISR running with antiprotons produced very high energy cross sections which could be compared with pp cross sections, there was impressive evidence that the difference cross section, $\sigma_{p\bar{p}} - \sigma_{pp}$, fell about as $s^{-1/2}$. The recent data confirm this. See. Fig. 7. This, however, does not rule out the possibility that the cross section difference might turn out to be asymptotically a small constant value, say a fraction of a millibarn. In fact, we have seen that in principle, if the cross section grows as $(\ln s)^2$, the difference cross section could grow as fast as $\ln s$. An even more subtle possibility is that the odd amplitude grows asymptotically as s, which according to our earlier discussion would be purely real (odd amplitudes go as $s^\alpha \exp[i\pi(1-\alpha)/2]$) and would thus not contribute to the total cross section, but would affect the ρ values.

To investigate such possibilities, we introduce [Łukaszuk and Nicolescu, 1973; Kang and Nicolescu, 1975; Joynson *et al.*,1975; Martin, 1982a]

$$\mathcal{M}_-^0 = E_-^0 s, \tag{37a}$$
$$\mathcal{M}_-^1 = E_-^1 s(\ln s/s_1 - i\pi/2), \tag{37b}$$
$$\mathcal{M}_-^2 = E_-^2 s(\ln s/s_1 - i\pi/2)^2, \tag{37c}$$

where the E's are real constants. We shall refer to the amplitudes in Eqs.(37) as Odderon-0, Odderon-1 and Odderon-2, respectively. The full odd amplitude is given by the sum, $\mathcal{M}_-^{tot}$ of $\mathcal{M}_-$ from Eq.(33), and one of the terms from Eq. (37). Odderon-0 affects the ρ values but not the cross sections, being entirely real. Odderon-1 gives a constant cross section difference, while Odderon-2 gives a cross section difference growing as $\ln s$.

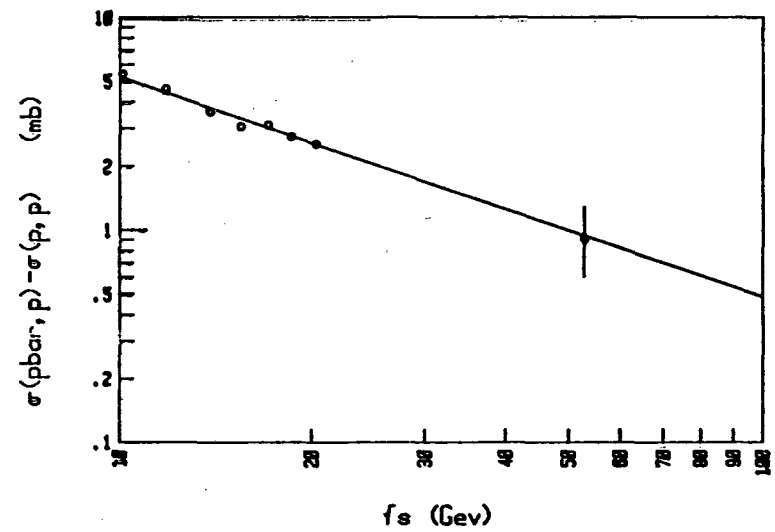

Fig. 7. The difference, $\sigma_{p\bar{p}} - \sigma_{pp}$ vs. $\sqrt{s}$. The curve is from Fit #3. See Eq. (34) and Table I. [Block and Cahn, 1982a]

If the scale, s_1, in Odderon-1 or Odderon-2 is too large, the magnitude of the amplitude may fall with increasing s, contrary to our intent in using this parameterization. To prevent this distortion, we constrain s_1 to be the same as s_0, the parameter in the even amplitude.

There is a theorem, due to Fischer and co-workers [Fischer *et al.*, 1978; Fischer, 1981] ,which states, in part, that if above some energy, the signs of $Im\mathcal{M}_-^{tot}$ and $Re\mathcal{M}_-^{tot}$ remain the same, then the difference of the cross sections tends to zero. Clearly this theorem is satisfied by the amplitude $\mathcal{M}_-$ of Eq. (33) for $0 < \alpha < 1$. The addition of an Odderon-1 or an Odderon-2 amplitude can be seen to lead to opposite signs for $Im\mathcal{M}_-^{tot}$ and $Re\mathcal{M}_-^{tot}$ in the limit of high s. This is of course in accord with the Fischer theorem, since these terms lead to non-vanishing cross section differences.

We have made three separate fits to the data using successively Odderon-0, Odderon-1, and Odderon-2. The results of these fits are shown in Table I. In all three cases, the value of E is about two standard deviations away from zero and there is thus no proven need for these amplitudes. It is of interest to examine quantitatively the limits that can be placed on their presence. For Odderon-0, an appropriate comparison is that between A and E, the coefficients of the purely imaginary odd amplitude and the purely real even amplitude with the same s-dependence. The magnitude of E is less than one percent of that of A. This is an impressive limit since this odd amplitude cannot contribute to the cross section. The limits on the other fits are comparable. Altogether, then, we conclude that these amplitudes which are allowed by analyticity, if present at all, are less than one percent as strong as the dominant portion of the forward scattering amplitude.

Using the values for Odderon-1 found in Table I, we note that

since D and E are both negative, $Re\mathcal{M}_-^{tot}$ is negative for $s > s_0$. On the other hand, $Im\mathcal{M}_-^{tot}$ is negative and dominated by $\mathcal{M}_-$ [Eq.(33)] at ISR energies. It does not change sign until $s^{1/2} = 200$GeV. Thus any attempt to invoke the Fischer theorem at present energies is premature. The corresponding sign change for the Odderon-2 would be at $s^{1/2} = 75$ GeV. Since these sign changes occur in $Im\mathcal{M}_-^{tot}$, they reflect a change in the sign of $\Delta\sigma = \sigma_{p\bar{p}} - \sigma_{pp}$. The existing data are thus compatible with such a sign change, and using Table I we extrapolate the Odderon-2 fit to $s^{1/2} = 540$ GeV, where we find $\sigma_{p\bar{p}} - \sigma_{pp} = -1.6 \pm 0.8$ mb. The unconventional sign of the difference is possible because the Odderon contributes oppositely to the amplitude $\mathcal{M}_-$, Eq. (33), which dominates the odd amplitude at lower energies. The magnitude of this difference and its uncertainty show clearly the desirability of making both pp and $p\bar{p}$ cross section measurements at collider energies. At the same time, these numbers provide a quantitative estimate of the required precision. The presence of Odderon-0 is especially difficult to detect experimentally. Data at very high energies would not particularly improve the situation. For example, using our values for Odderon-0 from Table I, we would predict $\Delta\rho = \rho_{pp} - \rho_{p\bar{p}}$ at $s^{1/2} = 540$ GeV to be 0.008 ± 0.003, whereas the fit without any Odderon gives $\Delta\rho = 0.0009 \pm 0.0002$ at the same s, a difference too small to be detected.

1.7 The Slope Parameter

In addition to the total cross section and ρ value, the nearly forward elastic scattering cross section has a third measurable feature, the slope parameter:

$$B(s,t) = \frac{d}{dt} \ln \frac{d\sigma}{dt}. \tag{38}$$

Frequently, it is the value at $t = 0$, $B(s) \equiv B(s, t = 0)$ which is of interest. For the simple amplitude of Eq.(11), $B(s)$ is the constant B. Back in the days when the total cross sections were believed to become constant asymptotically, the elastic scattering amplitude near the forward direction was parameterized as

$$\mathcal{M} \sim s^{\alpha(t)} e^{-i\pi\alpha(t)/2} e^{\beta t}, \tag{39}$$

where $\alpha(t) \approx 1 + \alpha'(0)t$ was the Pomeron trajectory, and β was a constant. In this model then

$$B(s) = 2\beta + 2\alpha'(0) \ln s. \tag{40}$$

Thus the canonical expectation was $B(s) \sim a \ln s + b$.

It is easy to see that this is not going to work if instead the cross section grows as $\ln^2 s$. If B is independent of t and the amplitude is purely imaginary, we can use Eq.(12):

$$\sigma_{el} = \frac{\sigma_{tot}^2}{16\pi B}, \tag{12}$$

We see that since σ_{el} cannot grow faster than $\ln^2 s$, certainly $B(s)$ must grow at least as fast as $\ln^2 s$ in the small t region.

Returning to our impact parameter representation

$$\mathcal{M} \sim s \int d^2b \exp(i\mathbf{q} \cdot \mathbf{b})\, a(b,s), \tag{41}$$

we expand about $q = 0$. Thus, if the phase of $a(b,s)$ is independent of b,

$$B(s) = \frac{\int db\, b^3 a(b,s)}{2 \int db\, b a(b,s)}. \tag{42}$$

This again shows that $B(s)$ measures the size of the proton.

We know that $a(b,s)$ must drop off for $b > b_c \sim \ln s$. It is surprising to learn that a form like

$$a(b,s) \sim \exp[-(b/b_c)^2], \tag{43}$$

is not permissible. Remember that even for imaginary q (if $|q|$ is small enough) this amplitude must be bounded by s^2. However, setting $q = iQ$ we find from Eqs.(41) and (43)

$$\mathcal{M} \sim s b_c^2 \exp(Q^2 b_c^2/4). \tag{44}$$

This grows faster than any power of s. We conclude that we need $a(b,s)$ to cut off very sharply, essentially as $a(b,s) = 0$ for $b > b_c$.

We can model this by supposing that $a(b,s) = \overline{a}(b/b_c)$ where $b_c = C \ln s$ and $\overline{a}(x) = 0$ for $x > 1$. Then

$$\mathcal{M} \sim s b_c^2 \int_0^1 dx\, x \overline{a}(x) J_0(q b_c x). \tag{45}$$

The remaining integral is an entire function of qb_c, that is it has no singularities in the finite qb_c plane. This is a consequence of the integral being confined to a finite range. Moreover, as qb_c goes to infinity, the amplitude grows no faster than exp(constant $\times$ qb_c). This result is a general one for total cross sections growing as $\ln^2 s$. We can state the conclusion by writing for the amplitude [Auberson, Kinoshita, and Martin, 1971]

$$\mathcal{M} \sim -is \ln^2 s f(t \ln^2 s), \tag{46}$$

where $f(z)$ is an entire function of order one-half, that is, for large $|z|$, $|f(z)|$ is bounded by $C \exp(C'|z|^{1/2})$ where C and C' are constants. This form is correct as $s \to \infty$. If t is fixed, then we see that

$$\begin{aligned} B(s,t) &< \frac{d}{dt} C'|t|^{1/2} \ln s \\ &< C'' \ln s. \end{aligned} \tag{47}$$

On the other hand, if we want the slope parameter at $t = 0$, we can expand Eq. (46) in powers of $t \ln^2 s$

$$\mathcal{M} \sim -is \ln^2 s[a + bt \ln^2 s + \cdots], \tag{48}$$

so that

$$B(s,0) \sim \ln^2 s. \tag{49}$$

This non-uniform behavior was discovered recently by Martin [Martin, 1982b]. As a practical matter, it still seems reasonable to use the form for $B(s,0)$ even at non-zero values of t since the other form, Eq.(47) is derived on the assumption that $t \ln^2 s$, or equivalently $t\sigma_{tot}$ is large.

On the basis of the above discussion, we choose to parameterize the amplitudes near the forward direction as [Block and Cahn, 1982b]

$$\mathcal{M}_+(s,t) = \mathcal{M}_+(s,0) \exp(b_+ t/2), \tag{50a}$$
$$\mathcal{M}_-(s,t) = \mathcal{M}_-(s,0) \exp(b_- t/2), \tag{50b}$$

where

$$b_+ = c_+ + d_+ \ln s + e_+ \ln^2 s, \tag{51a}$$
$$b_- = c_- + d_- \ln s, \tag{51b}$$

The amplitudes at $t = 0$ are just those in Eqs.(31) and (33) with $a = 0$ and $C = 0$, and the remaining parameters at $t = 0$ are fixed to be those of the first fit in Table I. The five parameters left to describe the slope are then fitted using the available data. Unfortunately, the data are not mutually consistent. However, with a suitable choice of data sets, the results are sensible, as shown in Fig. 8. The value of the slope parameter at $-t = 0.02\,\mathrm{GeV}^2$ is predicted to be $16.7 \pm 0.7\,\mathrm{GeV}^{-2}$ at the SPS collider energy, $s^{1/2} = 540$ GeV. The result reported by UA-4 is $17.2 \pm 1.0\,\mathrm{GeV}^{-2}$ at $-t = 0.05\,\mathrm{GeV}^2$ [UA4 Collaboration, 1982a].

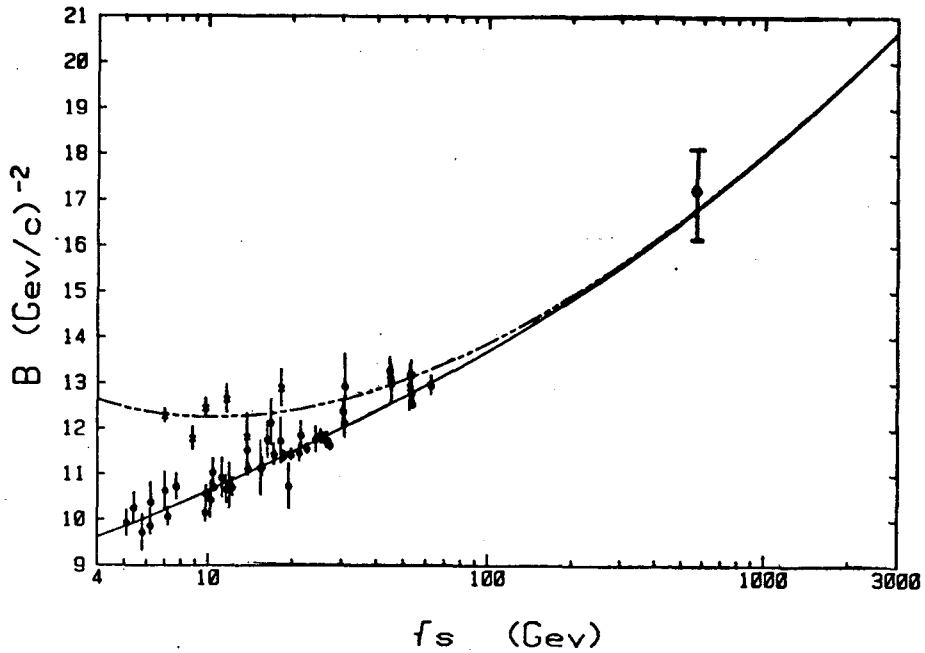

Fig. 8. The slope parameter, $B(s, t = -0.02\text{GeV}^2)$ vs. $\sqrt{s}$. The upper curve and data are for $p\bar{p}$ and the lower are for pp. [Block and Cahn, 1982b]

2. Hard Scattering Processes

2.1 Perspective

Quantum chromodynamics provides a means of analyzing hard scattering processes including the production of high transverse momentum jets, high invariant mass dilepton pairs, and heavy quarks. These processes are imagined to proceed through the scattering of partons (quarks and gluons). If we look only at this scattering process, which takes place in a volume of about 1 fm^3, perturbative QCD should be reliable (see Bjorken's SLAC Summer School Lectures of 1979 on QCD). It is conventional to view the full scattering event as having three stages: the breakdown of the initial hadrons into partonic constituents, the scattering of the partons, and the transformation of the final state partons into hadrons.

We shall adopt this view in an extreme form. We shall use the term "beam" to mean the flux of partons arising from the physical beam. The "scattering" will refer just to the partonic scattering event.By the "detector" we shall mean not just the physical apparatus, but also the space outside the tiny region - the "femto-universe" - in which the "scattering" occurs. Thus, for example, the hadron cascade inside a calorimeter and the hadronization of a high momentum quark will both be regarded as characteristics of the "detector". This is a description in keeping with Bj's notion that a really good detector would be able to detect quarks and gluons. Our inability to make such measurements will simply be regarded as a flaw in our detector. Of course, we may hope to compensate for this by obtaining a very complete understanding of our "detector", meaning that we may hope to find signatures that will identify the outgoing parton type and its momentum. Such an understanding would naturally require great advances both theoretically and experimentally.

This separation may seem perverse. It pushes off the difficult problems into the experimental factors: the "beam" and the "detector". In fact, this separation is dictated by QCD . The concept of "factorization" tells us that the infrared singularities we encounter in calculating can be relegated either to the process by which the initial hadron turns into partons (the "beam") or to the process by which the final partons become hadrons(in the "detector").

2.2 The Beam

For colliding beam machines, the fundamental equation is

$$Rate = \mathcal{L}\sigma, \tag{52}$$

where $\mathcal{L}$ is the luminosity. If the two physical beams have "transverse" densities (i.e. particles/cm^2) of $\rho_1(\mathbf{r})$ and $\rho_2(\mathbf{r})$, and cross n times per second, the luminosity is

$$\mathcal{L} = n \int d^2r\, \rho_1(\mathbf{r})\rho_2(\mathbf{r}). \tag{53}$$

For the CERN SPS collider, the design values of $\int d^2r\, \rho_1$ and $\int d^2r\, \rho_2$ are about 10^{11} with an effective area of $3 \times 10^{-3}\mathrm{cm}^2$. With six beam-beam collisions per cycle at each intersection point (that is, six bunches each of protons and anti-protons) and a machine radius of about 10^3 m, we have

$$n = \frac{6 \cdot 3 \cdot 10^8 \mathrm{m/s}}{2\pi \cdot 10^3 \mathrm{m}}, \tag{54}$$

and a design luminosity of $10^{30}\mathrm{cm}^{-2}\mathrm{sec}^{-1}$. The maximum luminosity achieved before July1, 1982 was about $1.8 \times 10^{28}\mathrm{cm}^{-2}\mathrm{sec}^{-1}$.

The "beams" we are concerned with are the beams of partons - quarks, anti-quarks, and gluons. These partons are not monochromatic of course. In fact, each proton carries a distribution of quarks and gluons which depends on x, the fraction of the proton's momentum carried by the parton: $f_i(x), (i = u, \overline{u}, \ldots g)$. This function is also weakly a function of the momentum transfer in the subprocess of interest (this dependence is called "scale breaking" or violation of " Bjorken scaling"). Ignoring this "Q^2" dependence for the moment, we ask what is the effective luminosity for, say, u-quarks on anti-u-quarks, per unit of center-of-mass energy squared (of the quark anti-quark system)? If we indicate the contributions from the two incident physical particles by the subscripts 1 and 2, we have

$$\frac{d\mathcal{L}_{u\overline{u}}}{d\hat{s}} = \int dx_1\, dx_2 \delta(\hat{s} - s x_1 x_2)[f_{1u}(x_1) f_{2\overline{u}}(x_2) + f_{1\overline{u}}(x_1) f_{2u}(x_2)], \tag{55}$$

where $\hat{s}$ is the parton-parton center of mass energy squared. Let us call $\tau = \hat{s}/s$ so that

$$\frac{d\mathcal{L}_{u\overline{u}}}{d\tau} = \int dx_1 dx_2 \delta(\tau - x_1 x_2)[f_{1u}(x_1) f_{2\overline{u}}(x_2) + f_{1\overline{u}}(x_1) f_{2u}(x_2)]. \tag{56}$$

The quantities $\frac{d\mathcal{L}_{u\overline{u}}}{d\tau}, \frac{d\mathcal{L}_{u\overline{d}}}{d\tau}, \ldots, \frac{d\mathcal{L}_{ug}}{d\tau}, \ldots, \frac{d\mathcal{L}_{gg}}{d\tau}$ are the fundamental characteristics of the "beam". The functions $f_u(x), f_d(x), \ldots, f_g(x)$ are determined by experiments including electroproduction and neutrinoproduction, and by theoretical considerations.

Some of these luminosity spectra have been calculated by Horgan and Jacob, 1981, and by Duke and Quigg, 1982. See Fig. 9. Their results

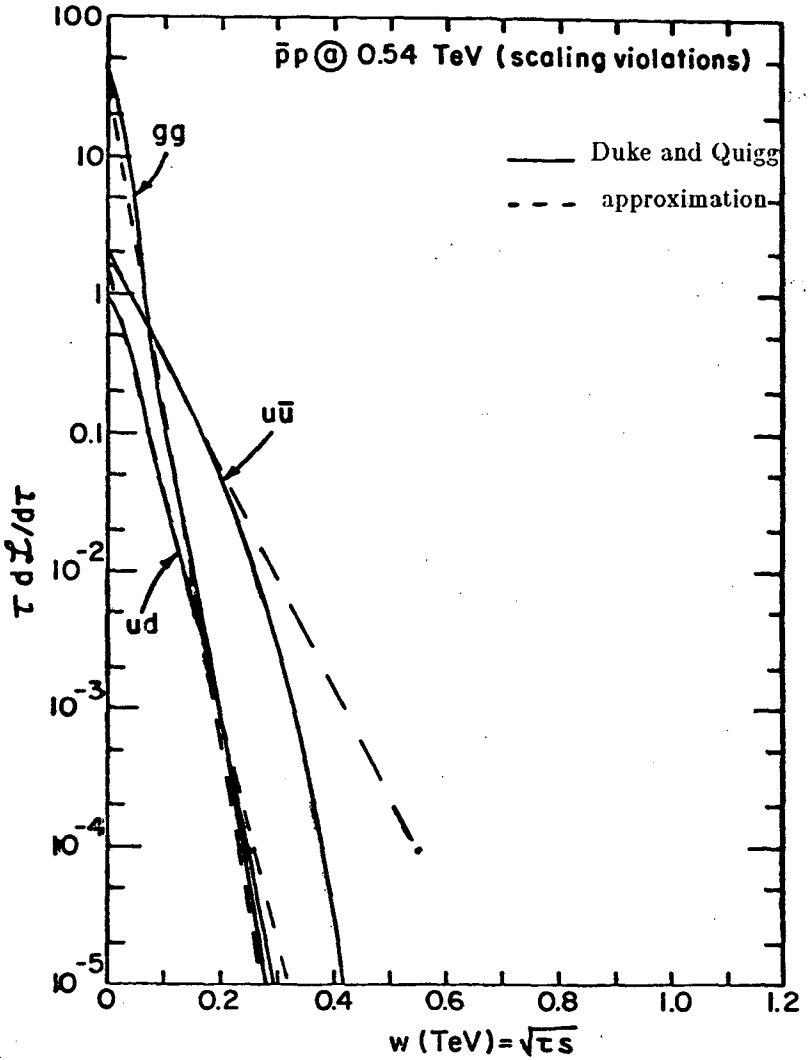

Fig. 9.a. The luminosity spectrum $\tau\frac{dL}{d\tau}$ vs. $W = \sqrt{\tau s}$ for $p\bar{p}$ collisions at $\sqrt{s} = 540\,\mathrm{GeV}$. The dashed lines are the approximations Eq.(57). [after Duke and Quigg, 1982]

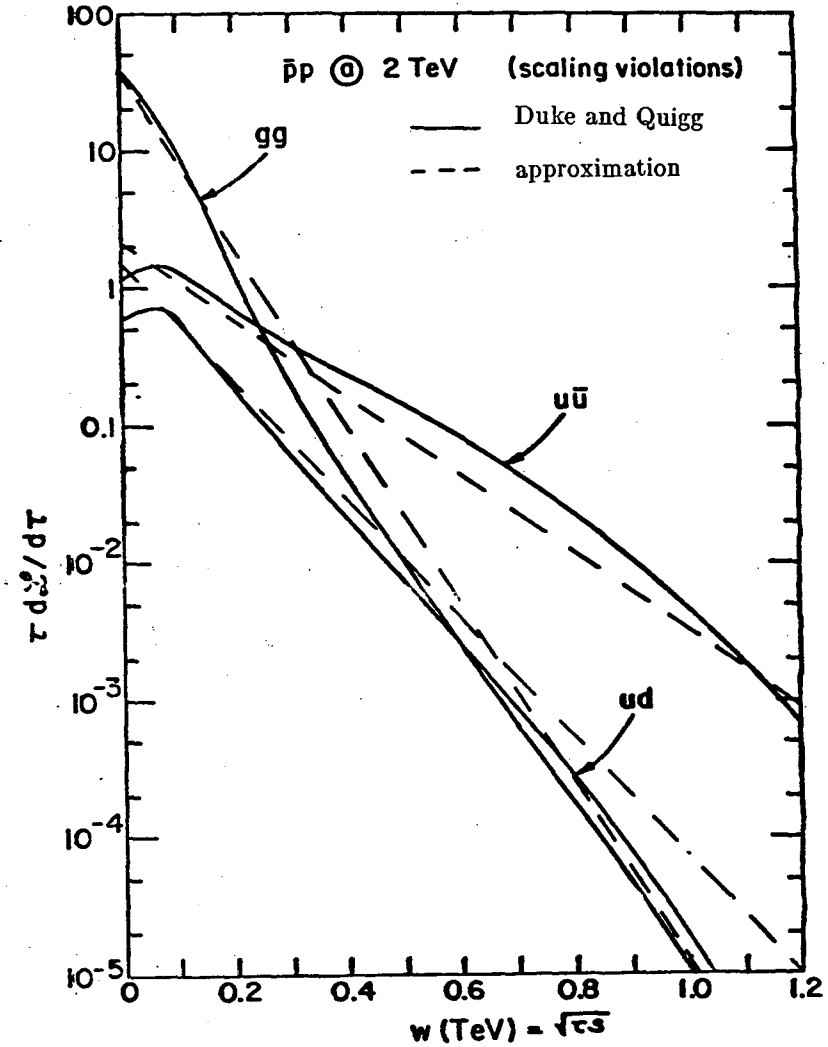

Fig. 9.b. The luminosity spectrum $\tau\frac{dL}{d\tau}$ vs. $W = \sqrt{\tau s}$ for $p\bar{p}$ collisions at $\sqrt{s} = 2000\,\mathrm{GeV}$. The dashed lines are the approximations Eq.(57). [after Duke and Quigg,1982]

can be approximated by analytic forms. For $p\bar{p}$ collisions at $s^{1/2} = 540\,\mathrm{GeV}$ we take

$$\begin{aligned}
\tau\frac{d\mathcal{L}_{u\bar{u}}}{d\tau} &= 2e^{-10\sqrt{\tau}} \\
\tau\frac{d\mathcal{L}_{uu}}{d\tau} &= 1.5e^{-20\sqrt{\tau}} \\
\tau\frac{d\mathcal{L}_{gg}}{d\tau} &= 40e^{-30\sqrt{\tau}} \\
\tau\frac{d\mathcal{L}_{ug}}{d\tau} &= 20e^{-20\sqrt{\tau}}
\end{aligned} \tag{57}$$

For simplicity, we have chosen forms with no scale breaking. It is apparent from Figs.(9.a) and (9.b) that this is an adequate approximation for the energy range between the CERN and Fermilab colliders.

When valence quarks are present (u and d in a proton, anti-u and anti-d in an antiproton), they dominate the distribution. Very roughly, in a proton, $f_u = 2f_d$. Thus for $p\bar{p}$ collisions, we take

$$\begin{aligned}
\frac{d\mathcal{L}_{u\bar{d}}}{d\tau} &\approx \frac{1}{2}\frac{d\mathcal{L}_{u\bar{u}}}{d\tau} \\
\frac{d\mathcal{L}_{d\bar{d}}}{d\tau} &\approx \frac{1}{4}\frac{d\mathcal{L}_{u\bar{u}}}{d\tau}
\end{aligned} \tag{58}$$

If we have a cross section $d\sigma$ for a partonic subprocess which depends on $\hat{s}$, we can find an effective cross section by integrating over τ:

$$d\sigma_{eff}(s) = \int d\tau \sum_{i,j} d\sigma_{ij}(\hat{s} = \tau s)\frac{d\mathcal{L}_{ij}}{d\tau}. \tag{59}$$

Here the sum is over the various parton types, i and j. We shall use this basic formula to estimate the cross sections for the important hard scattering processes.

2.3 Cross Sections

We first consider the production of high mass dilepton pairs in hadronic collisions. The partonic cross section is simply related to the usual $e^+e^- \to \mu^+\mu^-$ cross section at center of mass energy squared s,

$$\sigma = \frac{4\pi\alpha^2}{3s}. \tag{60}$$

The only change required is that we must take into account the charge of the annihilating quarks and their color. A quark and an anti-quark can annihilate only if they have opposite colors. Thus we use

$$\sigma(q\bar{q} \to \mu^+\mu^-) = \frac{1}{3}e_Q^2\frac{4\pi\alpha^2}{3s}, \tag{61}$$

where e_Q is the quark charge. The effective cross section is given then by

$$\frac{d\sigma_{eff}}{d\tau} = \frac{4\pi\alpha^2}{3\hat{s}}\frac{1}{3}\left[\frac{4}{9}\frac{d\mathcal{L}_{u\bar{u}}}{d\tau} + \frac{1}{9}\frac{d\mathcal{L}_{d\bar{d}}}{d\tau}\right]. \tag{62}$$

Using our approximations for the luminosity spectra, Eq. (57), we find

$$s\frac{d\sigma_{eff}}{d\tau} = \frac{4\pi\alpha^2}{9\tau}\left[\frac{17}{36}\cdot\frac{2e^{-10\sqrt{\tau}}}{\tau}\right]. \tag{63}$$

This is displayed in Fig. 10. As an example,we calculate the Drell-Yan cross section (i.e. $\mu^+\mu^-$ production) for $M^2 = 100\,\mathrm{GeV}^2$ at $s^{1/2} = 540\,\mathrm{GeV}$. Thus $\sqrt{\tau} = 0.0185$. From Fig. 10, we find $s d\sigma/d\tau = 5 \cdot 10^2$. Thus we estimate

$$\begin{aligned}\frac{d\sigma}{dM} &= 2M\frac{d\sigma}{s\,d\tau}\\ &= 20\ \mathrm{GeV}\cdot\frac{1}{(540\ \mathrm{GeV})^4}\cdot 5\cdot 10^2\cdot(0.389\,\mathrm{mb\ GeV}^2)\\ &= 0.5\cdot 10^{-34}\mathrm{cm}^2\,\mathrm{GeV}^{-1}. \end{aligned} \tag{64}$$

We can use our expression to compare the expected performance of the colliders at CERN ($s^{1/2} = 540\,\mathrm{GeV}$) and at Fermilab ($s^{1/2} = 2000\,\mathrm{GeV}$). Let us compare $d\sigma/dM$ at M=50 GeV. Referring back to Eqs.(63) and (64), we see that $d\sigma/dM \sim f(M)\exp(-10\sqrt{\tau})$ so that

$$\begin{aligned}\frac{(d\sigma/dM)_{FNAL}}{(d\sigma/dM)_{CERN}} &= e^{10(\sqrt{\tau}_{CERN}-\sqrt{\tau}_{FNAL})}\\ &= e^{10(0.093-0.025)}\\ &\approx 2. \end{aligned} \tag{65}$$

We can also make the comparison with CBA (née Isabelle) where $s^{1/2} = 800\,\mathrm{GeV}$, but where we must use the luminosity spectrum for uu in $p\bar{p}$ to represent the luminosity for $u\bar{u}$ in pp.

$$\frac{(d\sigma/dM)_{CBA}}{(d\sigma/dM)_{FNAL}} = \frac{1.5e^{-20\sqrt{\tau}}}{2e^{-10\sqrt{\tau}}} = \frac{1.5e^{-20\cdot\frac{50}{800}}}{2e^{-10\cdot\frac{50}{2000}}} = 0.3. \tag{66}$$

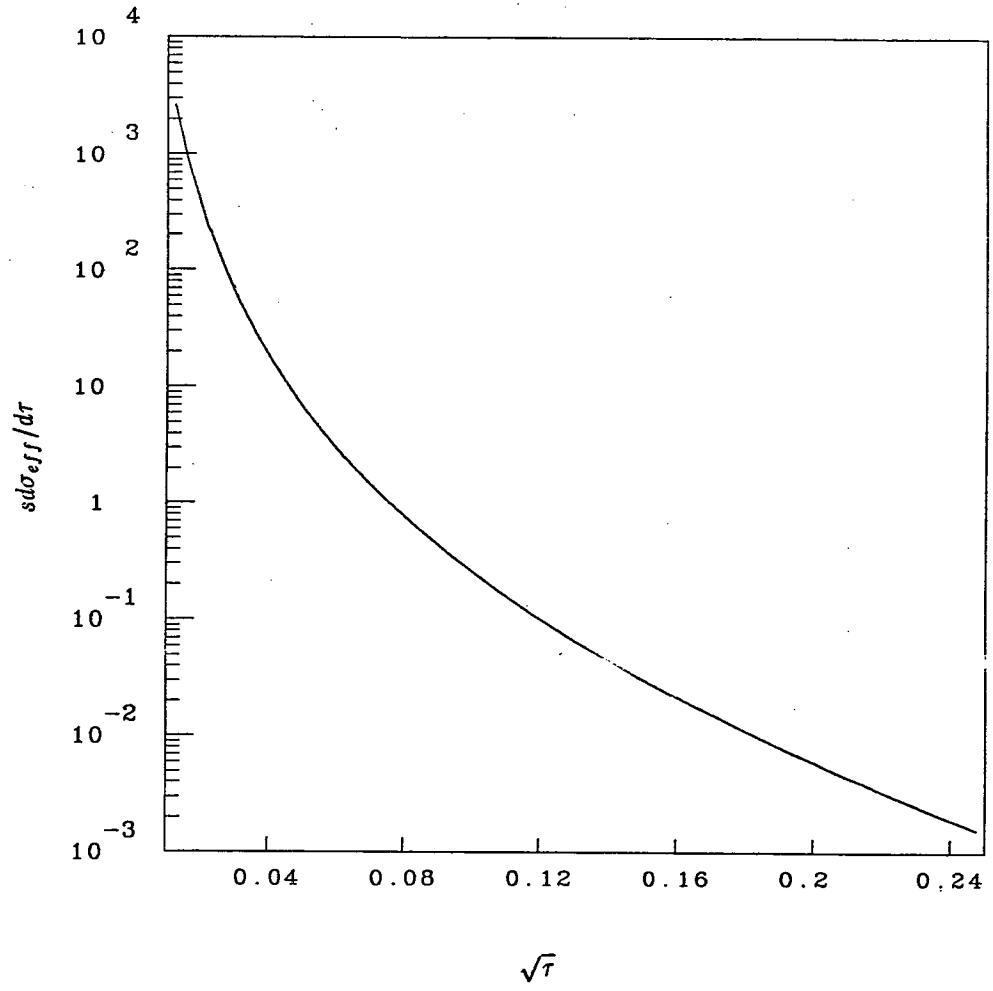

Fig. 10. The dimensionless Drell Yan cross section, $s d\sigma_{eff}/d\tau$ vs. $\sqrt{\tau}$. See Eq. (63).

CBA is the clear winner if it has, as designs suggest, 10^3 times the luminosity of the Tevatron collider. At a sufficiently high invariant mass, the Fermilab cross section makes up for the three orders of magnitude difference in luminosity. That mass is M = 330 GeV. This is too late. There are no events at this mass.

Just how large an invariant mass can we expect to reach? The cross section to produce a dilepton pair with $m_{\mu\mu} > m_0 = \sqrt{\tau_0 s}$ is, for $p\bar{p}$ machines

$$\sigma(m_{\mu\mu} > \sqrt{\tau_0 s}) = \int d\tau \frac{d\sigma_{eff}}{d\tau}, \tag{67}$$

$$= \frac{4\pi\alpha^2}{9s}\frac{17\cdot 2}{36}\int d\tau \frac{e^{-10\sqrt{\tau}}}{\tau^2}, \tag{68}$$

$$= 0.94\cdot 10^{-37}\,\mathrm{cm}^2\left(\frac{540\,\mathrm{GeV}}{\sqrt{s}}\right)^2 g(\tau_0), \tag{69}$$

where the function $g(\tau)$ is given by

$$g(\tau) = \frac{2}{\tau}E_3(10\sqrt{\tau}). \tag{70}$$

where $E_3(z)$ is an exponential integral [Abramowitz and Stegun, 1964, p.228]. The function $g(\tau)$ is shown in Fig. 11.

In the domain of interest to us, a simple but adequate approximation is

$$E_3(z) \approx \frac{1}{2}2^{-2z}, \tag{71}$$

so

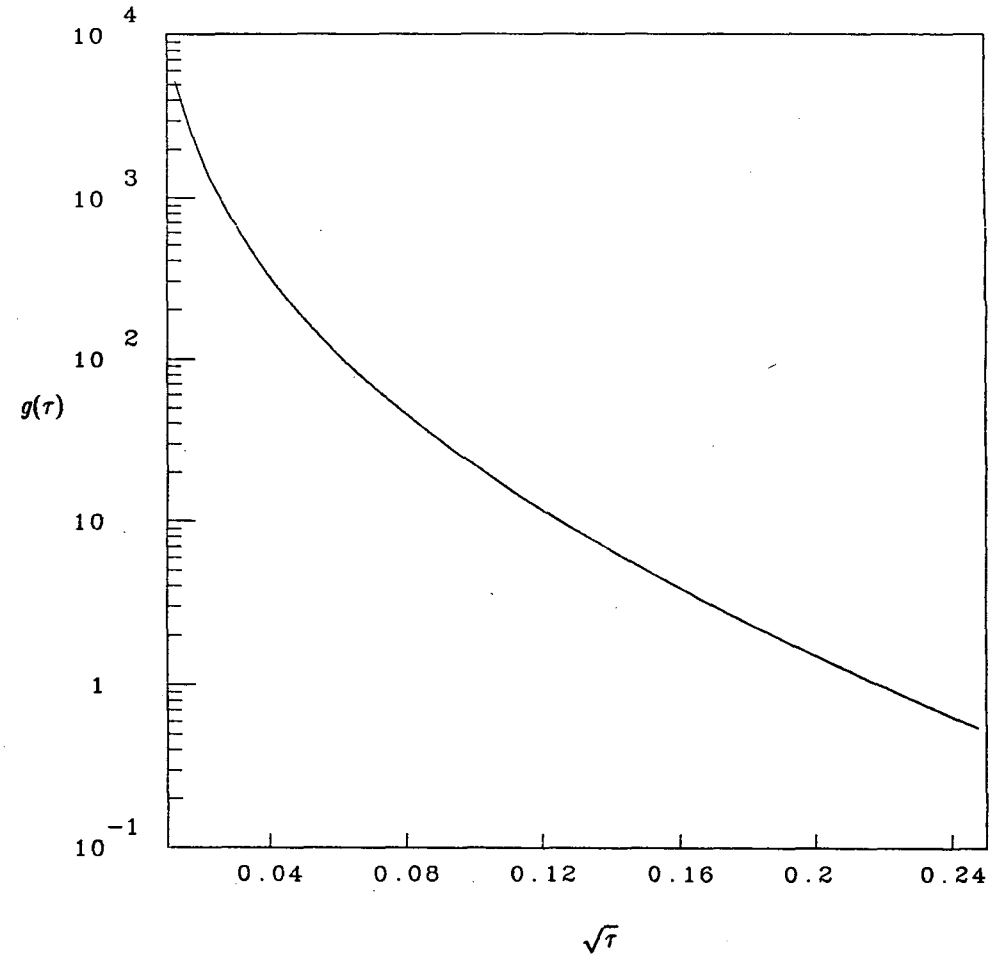

Fig. 11. The dimensionless function $g(\tau)$ vs. $\sqrt{\tau}$. See Eqs.(69), (70),and (72).

$$\sigma(m_{\mu\mu} > \sqrt{\tau_0 s}) \approx 10^{-37}\,\mathrm{cm}^2 \left(\frac{540\ \mathrm{GeV}}{\sqrt{s}}\right)^2 \frac{1}{\tau_0} 2^{-20\sqrt{\tau_0}}. \tag{72}$$

For $m_{\mu\mu} > 54$ GeV at the SPS collider, $\tau_0 = 0.01$ and $\sigma \approx 2.5 \cdot 10^{-36}\,\mathrm{cm}^2$. For $m_{\mu\mu} > 100$ GeV at the Fermilab collider, $\tau_0 = 0.0025$ and $\sigma = 1.5 \cdot 10^{-36}\,\mathrm{cm}^2$. These invariant masses are thus near the limit of what we may expect to see.

2.4 Resonance Production

We are especially interested in the production of W's and Z's, but without much extra effort we can find general expressions for the cross sections for production of any resonance in terms of its basic parameters. Naturally, we begin with the Breit-Wigner formula for the cross section for producing a resonance of mass M and width Γ. If the initial particles have spins S_1 and S_2, while the spin of the resonance is J, and if the branching ratio of the resonance into the initial channel is B, then

$$\sigma(\hat{s}) = \frac{\pi}{p_{cm}^2} \frac{2J+1}{(2S_1+1)(2S_2+1)} \frac{B\Gamma^2}{(\sqrt{\hat{s}} - M)^2 + (\Gamma/2)^2}. \tag{73}$$

The factor $(2S_1+1)(2S_2+1)$ is just the total number of initial spin orientations, which is four for two spin one-half particles. Actually, we must also use the value four if the two initial particles are massless vectors since the longitudinal degrees of freedom are missing. If the resonance is narrow, we can approximate Eq.(73) as

$$\sigma(\hat{s}) = \frac{2\pi^2}{p_{cm}^2} \frac{2J+1}{(2S_1+1)(2S_2+1)} B\Gamma\, \delta(\sqrt{\hat{s}} - M). \tag{74}$$

The effective cross section is obtained by integrating this cross section together with the luminosity spectrum:

$$\sigma_{eff} = \frac{4\pi^2}{M^2}(2J+1)B\frac{\Gamma}{M}\left(\tau\frac{d\mathcal{L}}{d\tau}\right)_{\tau=M^2/s}, \tag{75}$$

where we have taken the initial spin multiplicity to be four and assumed the incident particle (parton) masses are small compared to the resonance mass.

The expected properties of the Z and W are derived in Appendix A. The results are summarized in Table III. The branching ratio of the Z into a $u\bar{u}$ pair of a given color is 0.11/3 and into a $d\bar{d}$ pair is 0.13/3. In addition, we must multiply by a factor of 1/3 since only quarks with the proper color can annihilate. We can combine the $u\bar{u}$ and $d\bar{d}$ production if we assume the luminosity spectrum for $d\bar{d}$ is simply 1/4 of what it is for $u\bar{u}$. Putting all these factors together, we obtain an effective B:

$$B = \frac{1}{3}\left[\frac{0.11}{3} + \frac{1}{4}\cdot\frac{0.13}{3}\right] = 0.016. \tag{76}$$

At the CERN collider, we have for Z production, $\sqrt{\tau} = 0.17$, while at the Tevatron collider it will be 0.046. Thus we have using Eq.(57) for $\tau\frac{d\mathcal{L}_{u\bar{u}}}{d\tau}$

$$\sigma_{eff}(Z) = \frac{4\pi^2}{(92\mathrm{GeV})^2}(0.389\,\mathrm{mbGeV}^2)\cdot 3\cdot(0.016)\cdot\frac{2.8}{92}\begin{cases}0.37 & \text{CERN}\\ 1.3 & \text{FNAL}\end{cases}$$

Table III. Basic characteristics of the intermediate vector bosons according to the standard model with $\sin^2\theta_W = 0.21$.

	Z		W	
mass	92 GeV		81 GeV	
width	2.8 GeV		2.8 GeV	
branching ratios	e^+e^-	0.03	$e^+\nu_e$	0.08
	$\mu^+\mu^-$	0.03	$\mu^+\nu_\mu$	0.08
	$\tau^+\tau^-$	0.03	$\tau^+\nu_\tau$	0.08
	$\nu_e\overline{\nu}_e$	0.06		
	$\nu_\mu\overline{\nu}_\mu$	0.06		
	$\nu_\tau\overline{\nu}_\tau$	0.06		
	$u\overline{u}$	0.11	$u\overline{d}$	0.25
	$c\overline{c}$	0.11	$c\overline{s}$	0.25
	$t\overline{t}$	0.11	$t\overline{b}$	0.25
	$d\overline{d}$	0.13		
	$s\overline{s}$	0.13		
	$b\overline{b}$	0.13		

that is

$$\sigma_{eff}(Z) = 2.7\cdot 10^{-33}\mathrm{cm}^2 \times \begin{cases} 0.37 & \text{CERN} \\ 1.3 & \text{FNAL} \end{cases} \tag{77}$$

If we now include the sum of the branching ratios to e^+e^- and to $\mu^+\mu^-$ which is 0.06, we find cross sections into these modes of

$$\sigma_{eff}(p\overline{p} \to Z^0 + X \to \mu^+\mu^- \text{and} e^+e^- + X) = \begin{cases} 6\cdot 10^{-35}\mathrm{cm}^2 & \text{CERN} \\ 21\cdot 10^{-35}\mathrm{cm}^2 & \text{FNAL} \end{cases} \tag{78}$$

The cross section for W production is calculated analogously. The W^+ is produced by annihilation of a u and a $\overline{d}$.We take the luminosity for $u\overline{d}$ to be one-half the luminosity for $u\overline{u}$.The branching ratio of W^+ into $u\overline{d}$ of a single color is 1/12, which we again must divide by 3 to insure that the colliding quarks have the same color. Thus the effective value of B is 1/36. The value of $\sqrt{\tau}$ is 0.15 at CERN and 0.0405 at FNAL. We thus compute the cross section for W^+ production as

$$\sigma_{eff}(W^+) = \frac{4\pi^2}{(81\mathrm{GeV})^2}(0.389\,\mathrm{mbGeV}^2)\cdot 3\cdot \frac{1}{36}\frac{2.8}{81}\begin{cases} 0.22 & \text{CERN} \\ 0.67 & \text{FNAL} \end{cases}$$

$$= 6.7\cdot 10^{-33}\mathrm{cm}^2 \times \begin{cases} 0.22 & \text{CERN} \\ 0.67 & \text{FNAL} \end{cases} \tag{79}$$

If we insist on a leptonic decay of the W^+, we must add a factor of $1/6 = 1/12 + 1/12$ for the $e^+\nu$ and $\mu^+\nu$ modes. The result is

$$\sigma_{eff}(p\overline{p} \to W^+ + X \to \mu^+\nu \text{ and } e^+\nu) = \begin{cases} 2.5 \cdot 10^{-34}\text{cm}^2 & \text{CERN} \\ 7.5 \cdot 10^{-34}\text{cm}^2 & \text{FNAL} \end{cases}. \tag{80}$$

Of course there is an equal cross section for W^- production. The sum of the two is about one order of magnitude greater than that for the production of Z^0 with a subsequent decay into e^+e^- or $\mu^+\mu^-$.

The formula for the cross section for the production of a resonance has much broader applicability. Let us consider the production of p-wave quarkium (i.e. $Q\overline{Q}$) states by the collision of two gluons. The factor B should be set equal to 1/64 if we presume that gg is the only important channel. This is the product of one factor of 1/8 for the branching ratio into a single gluonic color channel and one factor of 1/8 to insure that the gluons colliding have the right colors to annihilate. For the width of the state, let us take 5 MeV, a figure representative of the values for the charmonium system. The spin of the produced resonance should be zero or two since two truly massless gluons cannot make a spin one state (by Yang's theorem). Thus 2J+1 is either one or five. Altogether then, we have for a resonance with a mass of 5 GeV

$$\begin{aligned} \sigma_{eff}(p\overline{p} \to P - state) &= \frac{4\pi^2}{(50\text{GeV})^2}(0.389\,\text{mbGeV}^2)\begin{Bmatrix} 1 \\ 5 \end{Bmatrix} \\ &\times \frac{1}{64}\frac{5 \cdot 10^{-3}}{50}\begin{cases} 2.5 & \text{CERN} \\ 19 & \text{FNAL} \end{cases} \\ &= 10^{-35}\text{cm}^2\begin{Bmatrix} 1 \\ 5 \end{Bmatrix}\begin{cases} 2.5 & \text{CERN} \\ 19 & \text{FNAL} \end{cases} \end{aligned} \tag{81}$$

While at first, the production of 1000 such particles in a standard run at Fermilab might sound encouraging, we must remember that the

only useful signature would be a cascade into an s-wave state followed by a decay into e^+e^- or $\mu^+\mu^-$. For simplicity, let us take as a guide, the branching ratios in the $c\overline{c}$ system. The 1982 Particle Data Booklet lists $B(\chi_2 \to \psi\gamma) = 0.157 \pm 0.017$ and $B(\psi \to e^+e^-) + B(\psi \to \mu^+\mu^-) = 0.148 \pm 0.012$. Thus we would expect about $1000 \times 0.15 \times 0.16 \approx 25$ events with a good signature. This appears to be observable since we estimate only eight Drell-Yan pairs above 50 GeV for the same standard run using Eq. (72). Increasing the mass of the resonance to 60 GeV decreases the yield by about 0.5 , and increasing it again to 70 GeV decreases it by an additional factor of 0.25 . There is no hope of finding quarkium above the Z mass this way.

2.5 High Transverse Momentum

We wish to use our ubiquitous formula

$$d\sigma_{eff} = \int d\tau \frac{d\mathcal{L}}{d\tau} d\sigma, \tag{82}$$

to estimate high transverse momentum jet cross sections. For the partonic cross sections we shall use the lowest order QCD results [Combridge, Kripfganz, and Ranft,1977; Cutler and Sivers, 1978; Owens, Reya, and Glück, 1978; Feynman, Field, and Fox, 1978]. This is not simply a consequence of laziness. As long as the problem of higher order QCD corrections to the Drell-Yan process is unresolved [Bodwin and Brodsky, 1981; Collins and Soper, 1982], it is pointless to take seriously QCD corrections for much more complicated processes. The lowest order differential cross sections for various partonic scattering processes are listed in Table IV and displayed in Fig. 12.

Table IV. Differential cross sections for partonic scattering. The differential cross section in the parton-parton center of mass is $d\sigma/d\Omega = (\alpha_s^2/4s)\Sigma$. The cross sections are color averaged and the expressions are derived from the results of Owens, Glück, and Reya, 1978 .

Process	Σ
$gg \to gg$	$18[(1-\cos\theta)^{-2}+(1+\cos\theta)^{-2}]$ $-9[(1-\cos\theta)^{-1}+(1+\cos\theta)^{-1}]$ $+99/8+(9/8)(\cos\theta)^2$
$gg \to q\bar{q}$	$(1/3)[(1-\cos\theta)^{-1}+(1+\cos\theta)^{-1}]$ $-(25/48)-(3/16)(\cos\theta)^2$
$q\bar{q} \to gg$	$(64/27)[(1-\cos\theta)^{-1}+(1+\cos\theta)^{-1}]$ $-(100/27)-(4/3)(\cos\theta)^2$
$gq \to gq$	$8(1-\cos\theta)^{-2}-4(1-\cos\theta)^{-1}$ $+(8/9)(1+\cos\theta)^{-1}+(11/9)$
$qq' \to qq'$	$(32/9)(1-\cos\theta)^{-2}-(16/9)(1-\cos\theta)^{-1}$ $+(4/9)$
$qq \to qq$	$(32/9)[(1-\cos\theta)^{-2}+(1+\cos\theta)^{-2}]$ $-(64/27)[(1-\cos\theta)^{-1}+(1+\cos\theta)^{-1}]+16/9$
$q\bar{q} \to q\bar{q}$	$(32/9)(1-\cos\theta)^{-2}-(32/27)(1-\cos\theta)^{-1}$ $+(2/9)$
$q\bar{q} \to q'\bar{q}'$	$(2/9)(1+(\cos\theta)^2)$

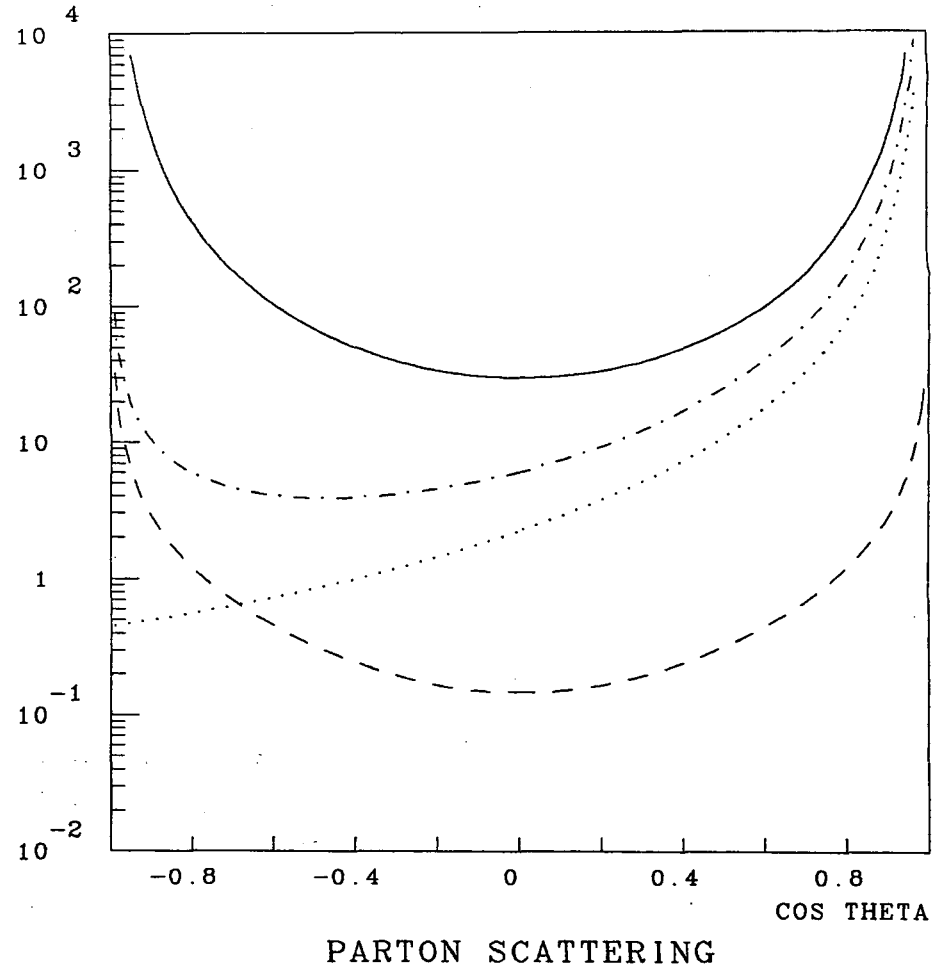

Fig. 12.a. The parton differential cross sections in the center of mass $(4s/\alpha_s^2)d\sigma/d\Omega$ vs. $\cos\theta$, $gg \to gg$(solid), $gg \to q\bar{q}$(dashed), $gq \to gq$(dot-dash), $qq' \to qq'$(dotted). Here q and q′ represent different flavors. The cross sections are color averaged.

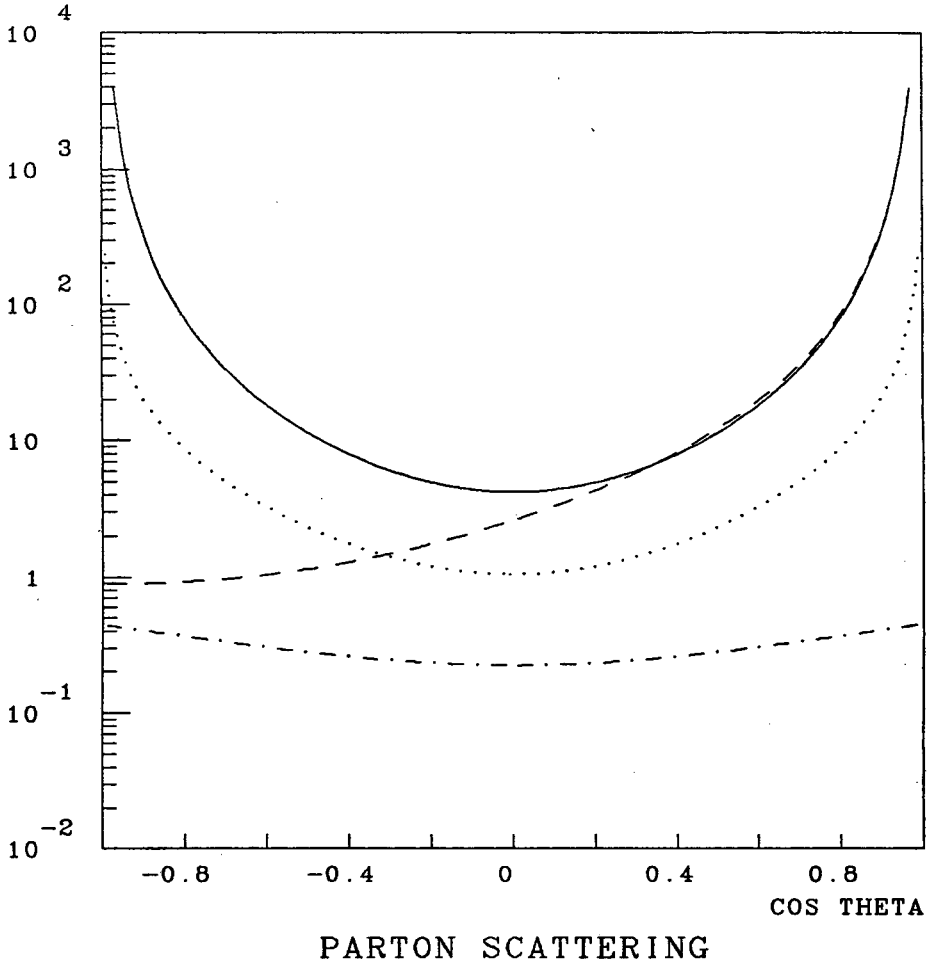

Fig. 12.b. The parton differential cross sections in the center of mass $(4s/\alpha_s^2)d\sigma/d\Omega$ vs. $\cos\theta$, $qq \to qq$(solid), $q\bar{q} \to q\bar{q}$(dashed), $q\bar{q} \to q'\bar{q}'$(dot-dash), $q\bar{q} \to gg$(dotted).

The quantity of physical interest is the differential cross section with respect to the transverse momentum of the jet, p_t. If the final state in the partonic scattering has unlike particles (i.e. all except $q\bar{q} \to gg, gg \to gg$ and $qq \to qq$), there are two contributions to consider: if a scattering angle θ gives a contribution, so does $\pi - \theta$. Thus we can add these two contributions and then restrict ourselves to scattering angles between 0 and $\pi/2$. We indicate this modified cross section by $d\bar{\sigma}/d\Omega$ and display it in Table V.

These differential cross sections are for the center of mass of the parton-parton system. The colliding partons have a momentum $\sqrt{\tau s}/2$ in this reference frame. Thus the center of mass scattering angle is related to the transverse momentum by

$$\sin\theta = \frac{2p_t}{\sqrt{\tau s}} = \frac{x_t}{\sqrt{\tau}}. \tag{83}$$

At fixed p_t, varying θ is equivalent to varying τ:

$$d\tau = \frac{2x_t^2 \cos\theta}{\sin^3\theta} d\theta. \tag{84}$$

On the other hand,

$$\frac{d\sigma}{dp_t} = \frac{2\pi}{p_t} \frac{\sin^2\theta}{\cos\theta} \frac{d\sigma}{d\Omega}, \tag{85}$$

so that

Table V. The differential cross section for partonic scattering with scattering angles between $\pi/2$ and π folded back to the region 0 to $\pi/2$. The differential cross section is given by $d\overline{\sigma}/d\Omega = (\alpha_s^2/4s)\overline{\Sigma}$.

Process	$\overline{\Sigma}$
$gg \to gg$	$18[(1-\cos\theta)^{-2}+(1+\cos\theta)^{-2}]$ $-9[(1-\cos\theta)^{-1}+(1+\cos\theta)^{-1}]$ $+99/8+(9/8)(\cos\theta)^2$
$gg \to q\overline{q}$	$(2/3)[(1-\cos\theta)^{-1}+(1+\cos\theta)^{-1}]$ $-(25/24)-(3/8)(\cos\theta)^2$
$q\overline{q} \to gg$	$(64/27)[(1-\cos\theta)^{-1}+(1+\cos\theta)^{-1}]$ $-(100/27)-(4/3)(\cos\theta)^2$
$gq \to gq$	$8[(1-\cos\theta)^{-2}+(1+\cos\theta)^{-2}]$ $-(28/9)[(1-\cos\theta)^{-1}+(1+\cos\theta)^{-1}]+(22/9)$
$qq' \to qq'$	$(32/9)[(1-\cos\theta)^{-2}+(1+\cos\theta)^{-2}]$ $-(16/9)[(1-\cos\theta)^{-1}+(1+\cos\theta)^{-1}]+8/9$
$qq \to qq$	$(32/9)[(1-\cos\theta)^{-2}+(1+\cos\theta)^{-2}]$ $-(64/27)[(1-\cos\theta)^{-1}+(1+\cos\theta)^{-1}]+16/9$
$q\overline{q} \to q\overline{q}$	$(32/9)[(1-\cos\theta)^{-2}+(1+\cos\theta)^{-2}]$ $-(32/27)[(1-\cos\theta)^{-1}+(1+\cos\theta)^{-1}]$ $+(4/9)+(4/9)(\cos\theta)^2$
$q\overline{q} \to q'\overline{q}'$	$(4/9)(1+(\cos\theta)^2)$

$$\frac{d\sigma_{eff}}{dp_t} = \int d\tau \frac{d\mathcal{L}}{d\tau}\frac{d\sigma}{dp_t} = \frac{4\pi}{p_t}\int d\theta \sin\theta \left(\tau\frac{d\mathcal{L}}{d\tau}\right)\frac{d\overline{\sigma}}{d\Omega}. \tag{86}$$

In principle, this integral goes from $\pi/2$ from $\sin^{-1} x_t$ but it is not a bad approximation to let the lower limit be zero since this extends the range of τ to $\tau = 1$ where the luminosity spectrum is very small anyway.

To proceed further, we need to make some assumptions about the luminosity spectrum. Rather than use the particular values given in Eq.(6), let us simply assume a parameterization

$$\tau\frac{d\mathcal{L}}{d\tau} = Ae^{-b\sqrt{\tau}}, \tag{87}$$

so that our results will be useful even if we want to vary A or b to consider another parameterization of the parton distributions, as might be appropriate at very much higher energies, say. Our general formula is thus

$$\frac{d\sigma}{dp_t} = \frac{4\pi}{p_t}\int_0^{\pi/2} d\theta \sin\theta A e^{-bx_t/\sin\theta}\frac{\alpha_s^2}{16p_t^2}\sin^2\theta\,\overline{\Sigma}(\theta) = \frac{\pi A}{4p_t^3}\alpha_s^2\int_0^{\pi/2} d\theta \sin^3\theta e^{-bx_t/\sin\theta}\,\overline{\Sigma}(\theta). \tag{88}$$

The values of the functions $\overline{\Sigma}$ for the various fundamental partonic processes are given in Table V. It is useful to define the dimensionless integrals

$$g_{qq\to qq}(z) = \int_0^{\pi/2} d\theta \sin^3\theta e^{-z/\sin\theta} \overline{\Sigma}_{qq\to qq}(\theta), etc. \tag{89}$$

which can, in fact, be done analytically in terms of modified Bessel functions and the like. Some representative values for these functions are given in Table VI and shown in Fig. 13.

In terms of these

$$\frac{d\sigma_{eff}}{dp_t} = \frac{\pi A}{4p_t^3}\alpha_s^2 g(bx_t). \tag{90}$$

For example, consider jets with $p_t = 27\,\mathrm{GeV}$ at the SPS collider. The contribution from the subprocess $gg \to gg$ is determined by noting that $x_t = 0.1$ and inserting the values (see Eq.(6)) b=30, A=40, and the nominal value $\alpha_s = 0.2$ to find, using Table VI,

$$g_{gg\to gg}(3) = 1.3,$$

and

$$\begin{aligned}\frac{d\sigma_{eff}}{dp_t} &= \frac{\pi\cdot 40}{4(27\mathrm{GeV})^3}\cdot(0.2)^2\cdot 1.3(0.389\mathrm{mbGeV}^2)\\ &= 3.2\cdot 10^{-32}\mathrm{cm}^2\mathrm{GeV}^{-1}.\end{aligned} \tag{91}$$

For small x_t, $gg \to gg$ dominates jet production, but at high enough x_t, $q\overline{q} \to q\overline{q}$ dominates in $p\overline{p}$ collisions. We can estimate that value of x_t as follows: For large bx_t, from Eq.(89),

$$g(bx_t) \approx \overline{\Sigma}(90^o)\sqrt{\frac{\pi}{2bx_t}}e^{-bx_t}. \tag{92}$$

Table VI. Values of the functions g(z) for $z = 0.1 - 4.$ used to determine $d\sigma/dp_t$ for hard scattering processes. See Eqs.(89)-(90).

z	0.1	0.2	0.4	1.	2.	4.
$gg \to gg$	140	90	50	18	4	0.4
$gg \to q\overline{q}$	0.5	0.4	0.3	0.1	0.04	0.004
$gq \to gq$	60	40	24	8	2	0.2
$qq' \to qq'$	26	17	10	3	0.8	0.07
$qq \to qq$	25	17	10	3	0.7	0.06
$q\overline{q} \to q\overline{q}$	27	18	11	4	0.8	0.07
$q\overline{q} \to q'\overline{q}'$	0.3	0.3	0.2	0.1	0.04	0.004
$q\overline{q} \to gg$	1.7	1.5	1.1	0.5	0.13	0.013

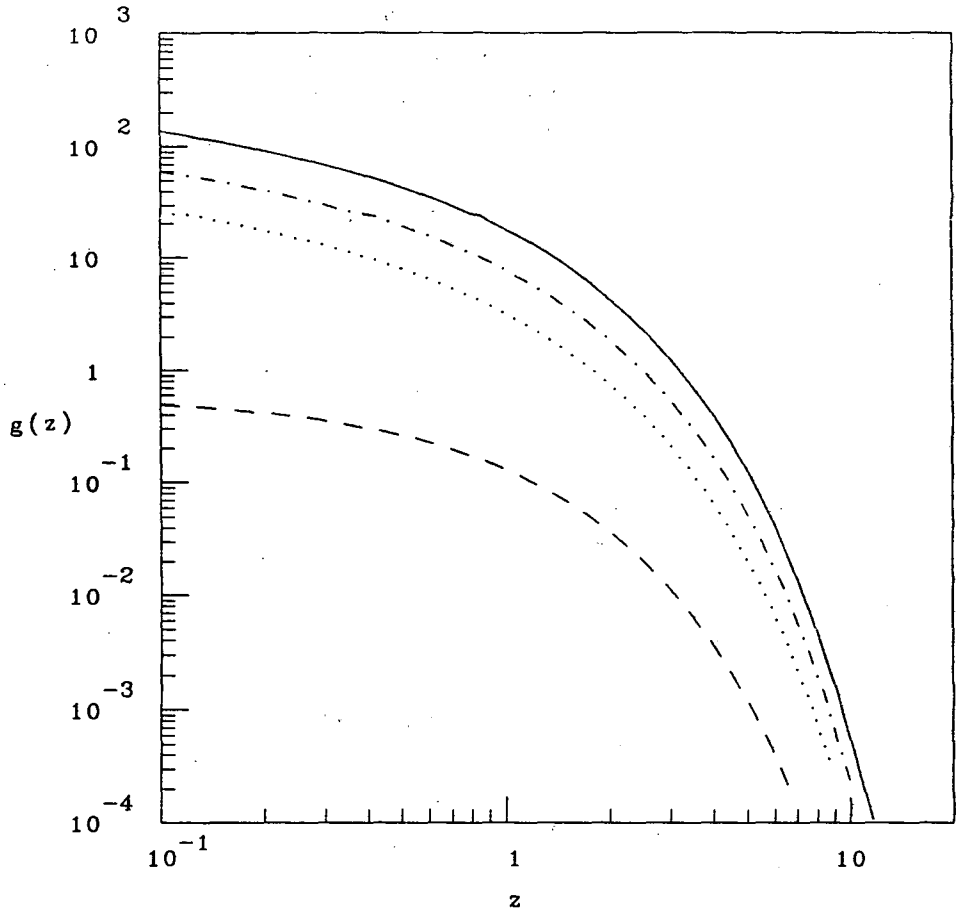

Fig. 13.a. The functions g(z), Eq. (89), vs. z for $gg \to gg$(solid), $gg \to q\bar{q}$(dashed), $gq \to gq$(dot-dash), and $qq' \to qq'$(dotted).

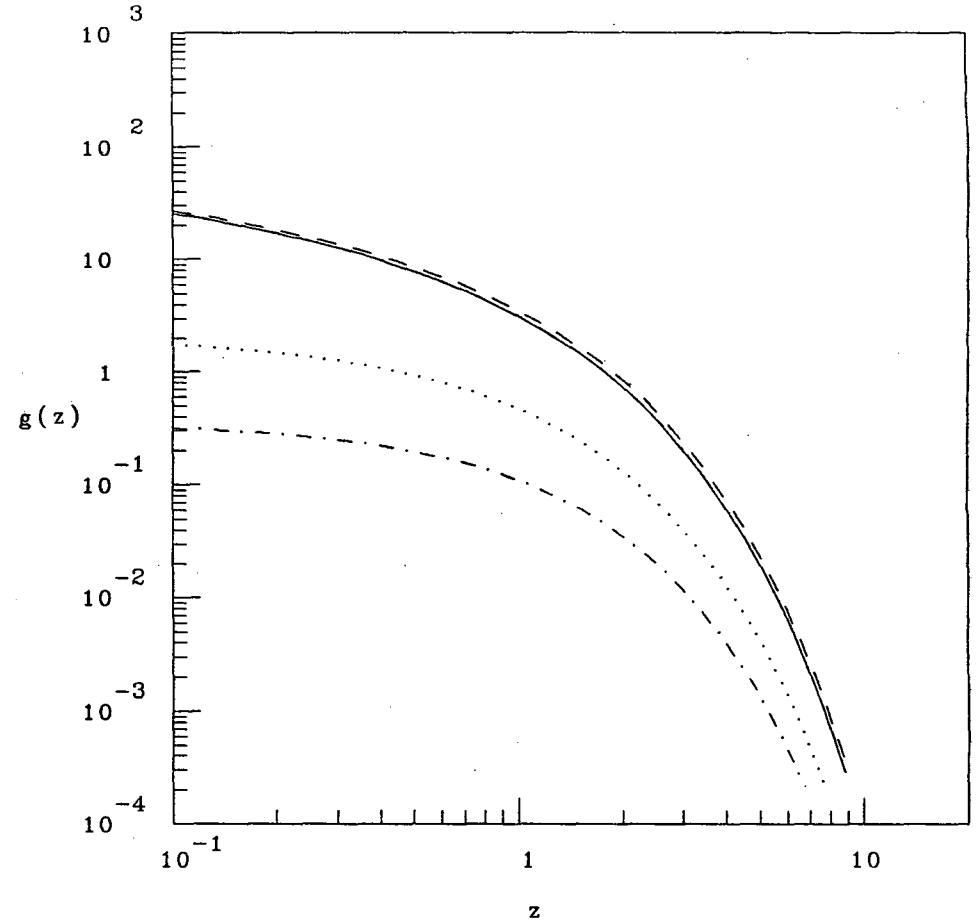

Fig. 13.b. The functions g(z), Eq. (89), vs. z for $qq \to qq$(solid), $q\bar{q} \to q\bar{q}$(dashed), $q\bar{q} \to q'\bar{q}'$(dot-dash), and $q\bar{q} \to gg$(dotted).

Now

$$\frac{d\sigma_{eff}}{dp_t} \sim Ag(bx_t), \tag{93}$$

so

$$\begin{aligned}\frac{(d\sigma_{eff}/dp_t)_{gg\to gg}}{(d\sigma_{eff}/dp_t)_{q\bar{q}\to q\bar{q}}} &= \frac{A_{gg\to gg}}{A_{q\bar{q}\to q\bar{q}}}\frac{\overline{\Sigma}_{gg\to gg}}{\overline{\Sigma}_{q\bar{q}\to q\bar{q}}}\sqrt{\frac{b_{q\bar{q}\to q\bar{q}}}{b_{gg\to gg}}}e^{(b_{q\bar{q}\to q\bar{q}}-b_{gg\to gg})x_t} \\ &\approx \frac{40}{2}\frac{30}{5}\sqrt{\frac{1}{3}}e^{-20x_t} \\ &\approx 70e^{-20x_t}\end{aligned} \tag{94}$$

This is unity if $x_t \approx 0.21$.

The cross section to produce a pair of jets, each with $x_t > x_{t0}$ is

$$\begin{aligned}\sigma(x_{t0}) &= \frac{\pi A\alpha_s^2}{s}\int_{x_{t0}}^{\infty} dx_t \frac{1}{x_t^3}g(bx_t) \\ &= \frac{\pi A\alpha_s^2 b^2}{s}\int_{bx_{t0}}^{\infty} du\frac{1}{u^3}g(u) \\ &\equiv \frac{\pi A\alpha_s^2 b^2}{s}h(bx_{t0})\end{aligned} \tag{95}$$

The functions h(z) for the various processes are displayed in Table VII and Fig. 14. For example, the cross sections for producing jets through $gg \to gg$, $gu \to gu$, and $u\bar{u} \to u\bar{u}$ at the Fermilab collider with $p_t >$ 100 GeV are calculated as follows:

Table VII. Selected values of the functions h(z) ,for $z = 0.1 - 4.$, used to determine the cross section to produce a jet with greater than a given value of the transverse momentum. See Eq.(95).

z	0.1	0.2	0.4	1.	2.	4.
$gg \to gg$	$3.4 \cdot 10^4$	$2.9 \cdot 10^3$	$2.2 \cdot 10^2$	6	$2.3 \cdot 10^{-1}$	$4 \cdot 10^{-3}$
$gg \to q\bar{q}$	$1.2 \cdot 10^3$	$1.3 \cdot 10^1$	1.2	$4 \cdot 10^{-2}$	$2 \cdot 10^{-3}$	$3 \cdot 10^{-5}$
$gq \to gq$	$1.5 \cdot 10^4$	$1.3 \cdot 10^3$	$1 \cdot 10^2$	2.5	0.1	$1.5 \cdot 10^{-3}$
$qq' \to qq'$	$6 \cdot 10^3$	$5 \cdot 10^2$	$4 \cdot 10^1$	1	$4 \cdot 10^{-2}$	$6 \cdot 10^{-4}$
$qq \to qq$	$6 \cdot 10^3$	$5 \cdot 10^2$	$4 \cdot 10^1$	1	$4 \cdot 10^{-2}$	$5 \cdot 10^{-4}$
$q\bar{q} \to q\bar{q}$	$7 \cdot 10^3$	$6 \cdot 10^2$	$4 \cdot 10^1$	1	$4 \cdot 10^{-2}$	$7 \cdot 10^{-4}$
$q\bar{q} \to q'\bar{q}'$	$8 \cdot 10^1$	9	0.9	$4 \cdot 10^{-2}$	$2 \cdot 10^{-3}$	$4 \cdot 10^{-5}$
$q\bar{q} \to gg$	$4 \cdot 10^2$	$5 \cdot 10^1$	4	0.2	$7 \cdot 10^{-3}$	$1 \cdot 10^{-4}$

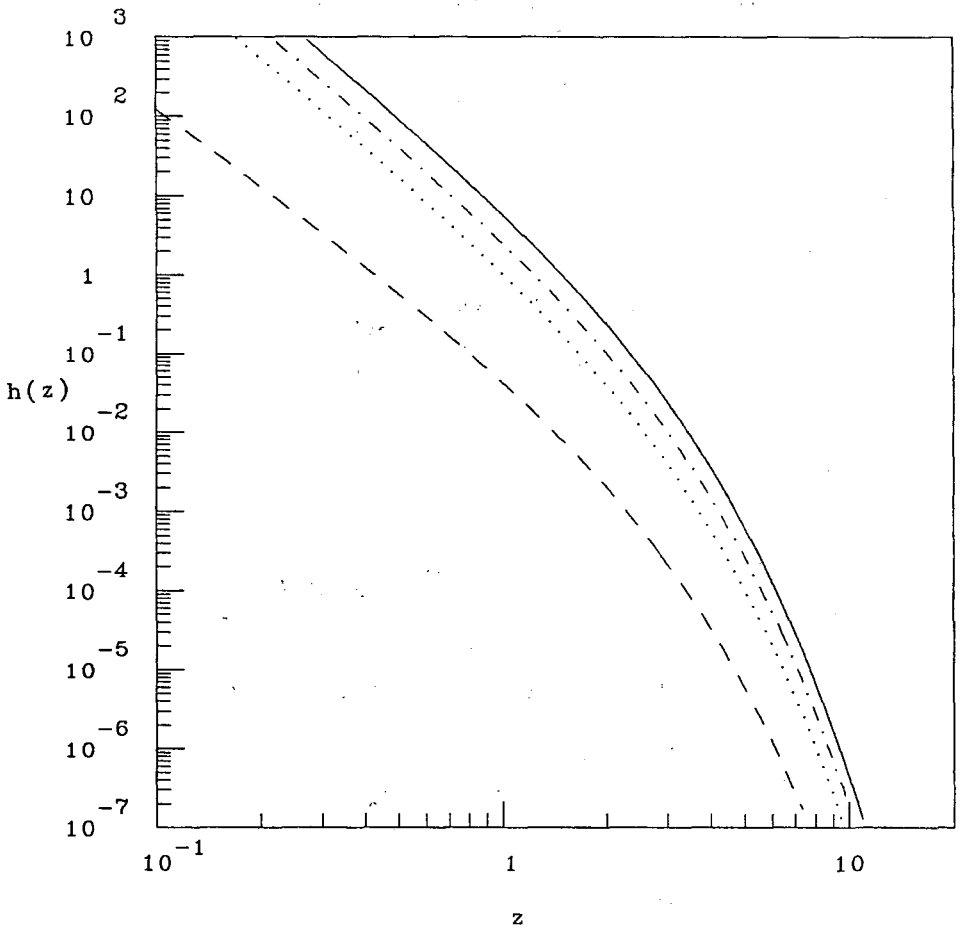

Fig. 14.a. The functions h(z), Eq. (89), vs. z for $gg \to gg$(solid), $gg \to q\bar{q}$(dashed), $gq \to gq$(dot-dash), and $qq' \to qq'$(dotted).

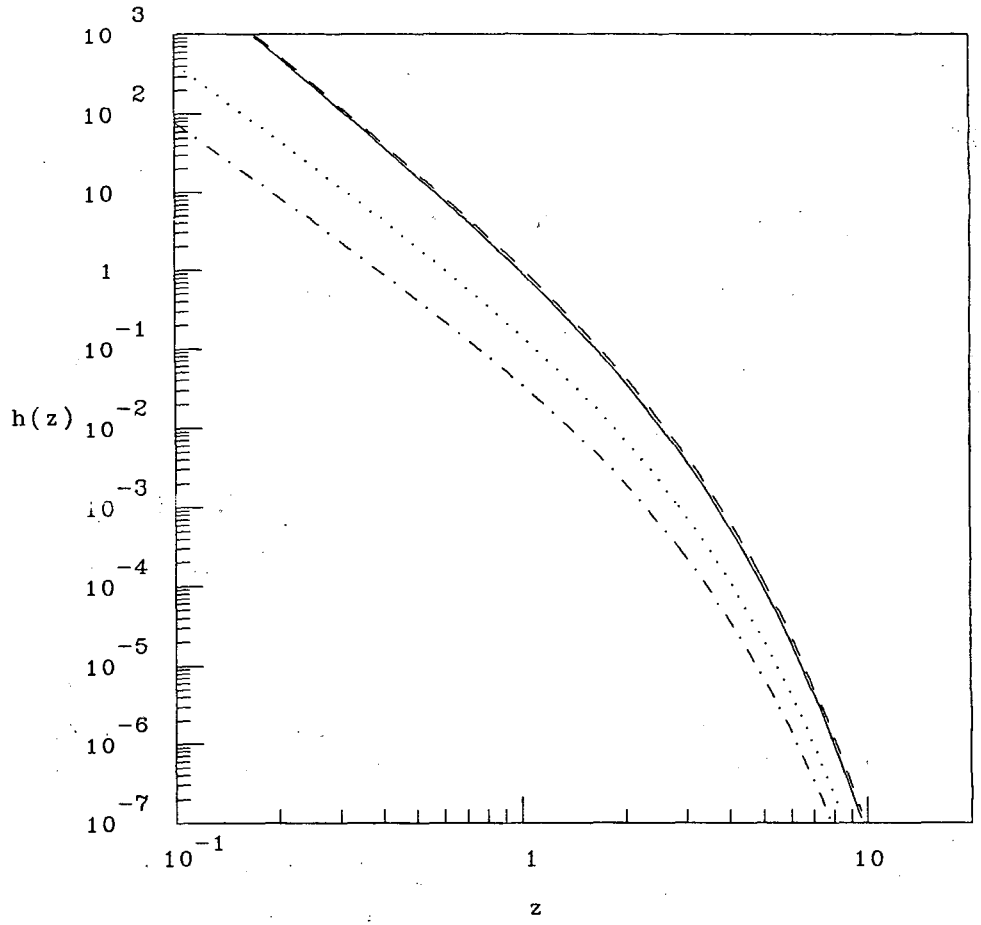

Fig. 14.b. The functions h(z), Eq. (89), vs. z for $qq \to qq$(solid), $q\bar{q} \to q\bar{q}$(dashed), $q\bar{q} \to q'\bar{q}'$(dot-dash), and $q\bar{q} \to gg$(dotted).

$$gg \to gg: \; A = 40, b = 30, x_t = 0.1, h_{gg\to gg}(3) = 4 \cdot 10^{-2}$$

$$\sigma = \frac{\pi \cdot 40 \cdot (0.2)^2 30^2}{(2000\,\mathrm{GeV})^2} 0.389\mathrm{mb\,GeV}^2 \cdot 0.04 = 1.8 \cdot 10^{-32}\mathrm{cm}^2$$

$$gu \to gu: \; A = 20, b = 20, x_t = 0.1, h_{gq\to gq}(2) = 0.1$$

$$\sigma = \frac{\pi \cdot 20 \cdot (0.2)^2 20^2}{(2000\,\mathrm{GeV})^2} 0.389\mathrm{mb\,GeV}^2 \cdot 0.1 = 1.0 \cdot 10^{-32}\mathrm{cm}^2$$

$$u\overline{u} \to u\overline{u}: A = 2, b = 10, x_t = 0.1, h_{q\overline{q}\to q\overline{q}}(1) = 1.$$

$$\sigma = \frac{\pi \cdot 2 \cdot (0.2)^2 10^2}{(2000\,\mathrm{GeV})^2} 0.389\,\mathrm{mb\,GeV}^2 \cdot 1. = 0.25 \cdot 10^{-32}\,\mathrm{cm}^2$$

For large values of bx_t there is a simple approximation for h(z) based on Eq. (92):

$$\begin{aligned} h(z) &\approx \int_z^\infty du \overline{\Sigma}(90^o) \sqrt{\frac{\pi}{2u}} \frac{1}{u^3} e^{-u} \\ &\approx \overline{\Sigma}(90^o) \sqrt{\frac{\pi}{2}}\, z^{-7/2}\, e^{-z}. \end{aligned} \tag{96}$$

Inserting this into Eq. (95) we have

$$\sigma(x_t > x_{t0}) \approx \frac{\pi A \alpha_s^2 b^2}{s} \overline{\Sigma}(90^o) \sqrt{\frac{\pi}{2}}\, (bx_{t0})^{-7/2} e^{-bx_{t0}}. \tag{97}$$

For $u\overline{u}$ in $p\overline{p}$ colllisions or uu in pp collisions, $A = 2, b = 10, \overline{\Sigma}(90^o) \approx 5$, so

$$\sigma(x_t > x_{t0}) \approx 6.6 \cdot 10^{-35}\mathrm{cm}^2 \left(\frac{540\,\mathrm{GeV}}{\sqrt{s}}\right)^2 x_{t0}^{-7/2} e^{-10x_{t0}}. \tag{98}$$

For example, the cross section at the Fermilab collider $p_t = 300$GeV or more from such $u\overline{u}$ collisions should be about $16 \cdot 10^{-36}\mathrm{cm}^2$.

2.6 Heavy Flavor Production

A number of mechanisms have been suggested for heavy flavor production. One obvious possibility is $q\overline{q} \to Q\overline{Q}$. Another is $gg \to Q\overline{Q}$. Of course, at a minimum the effects of the heavy quark mass, m_Q, must be retained in our QCD analysis. Although the naive predictions based on these processes are not especially successful, we shall restrict ourselves to this approach since it fits with the unified presentation of hard processes given above. While the absolute cross section predictions may not be accurate (even by the lax standards we believe are appropriate for the predictions in the previous sections), the general dependence on the center of mass energy may not be too far from the truth.

We begin then with the cross sections calculated by Combridge(1979)

$$\sigma_{q\bar{q}\to Q\bar{Q}} = \frac{8\pi\alpha_s^2}{27\pi}\left(1+\frac{2m_Q^2}{s}\right)\sqrt{1-\frac{4m_Q^2}{s}},$$

$$\sigma_{gg\to Q\bar{Q}} = \frac{\pi\alpha_s^2}{3s}\left[\left(1+\frac{4m_Q^2}{s}+\frac{m_Q^4}{s^2}\right)\ln\frac{1+\chi}{1-\chi}-\frac{1}{4}\chi\left(7+\frac{31m_Q^2}{s}\right)\right], \quad (99)$$

where

$$\chi = \sqrt{1-\frac{4m_Q^2}{s}}. \quad (100)$$

Let us write

$$\sigma_{q\bar{q}\to Q\bar{Q}}(\hat{s}) = \frac{\pi\alpha_s^2}{3s}F_{q\bar{q}}(\frac{\hat{s}}{4m_Q^2}), \quad (101)$$

$$\sigma_{gg\to Q\bar{Q}}(\hat{s}) = \frac{\pi\alpha_s^2}{3s}F_{gg}(\frac{\hat{s}}{4m_Q^2}). \quad (102)$$

Then in this model, the total heavy flavor production is

$$\sigma_{Q\bar{Q}} = \frac{\pi\alpha_s^2}{3s}\int d\tau\left(\tau\frac{d\mathcal{L}}{d\tau}\right)\frac{1}{\tau^2}\begin{cases}F_{q\bar{q}}(s\tau/4m_Q^2)\\ F_{gg}(s\tau/4m_Q^2)\end{cases}, \quad (103)$$

$$\sigma_{Q\bar{Q}} = \frac{\pi\alpha_s^2 A}{12m_Q^2}\int_1^\infty du\frac{1}{u^2}\exp(-b\sqrt{4m_Q^2u/s})\begin{cases}F_{q\bar{q}}(u)\\ F_{gg}(u)\end{cases}, \quad (104)$$

where

$$u = s\tau/4m_Q^2, \quad (105)$$

and where

$$F_{q\bar{q}}(u) = \frac{8}{9}\left(1+\frac{1}{2u}\right)\sqrt{1-\frac{1}{u}}, \quad (106)$$

$$F_{gg}(u) = \left(1+\frac{1}{u}+\frac{1}{16u^2}\right)\ln\frac{1+\chi}{1-\chi}-\frac{1}{4}\chi\left(7+\frac{31}{4u}\right), \quad (107)$$

$$\chi = \sqrt{1-\frac{1}{u}}. \quad (108)$$

Having reduced the problem to quadrature, we can simply do the integrals numerically to find

$$G_{q\bar{q}}(z) = \int_1^\infty du\, e^{-z\sqrt{u}}\frac{1}{u^2}F_{q\bar{q}}(u),$$

$$G_{gg}(z) = \int_1^\infty du\, e^{-z\sqrt{u}}\frac{1}{u^2}F_{gg}(u), \quad (109)$$

in terms of which

$$\sigma_{Q\bar{Q}}(s) = \frac{\pi\alpha_s^2 A}{12m_Q^2}\begin{cases}G_{q\bar{q}}\left(b\sqrt{4m_Q^2/s}\right)\\ G_{gg}(b\sqrt{4m_Q^2/s})\end{cases} \quad (110)$$

The functions $F_{q\bar{q}}$ and F_{gg} are shown in Fig. 15. At high energy (i.e. large u), the gg mechanism is more effective since it is suppressed only by the t-channel exchange of the heavy quark, rather than the s-channel single gluon pole. The integrated functions, $G_{q\bar{q}}$ and G_{gg} , are shown in Fig. 16. As $z \to 0$, these functions approach constant values, so as

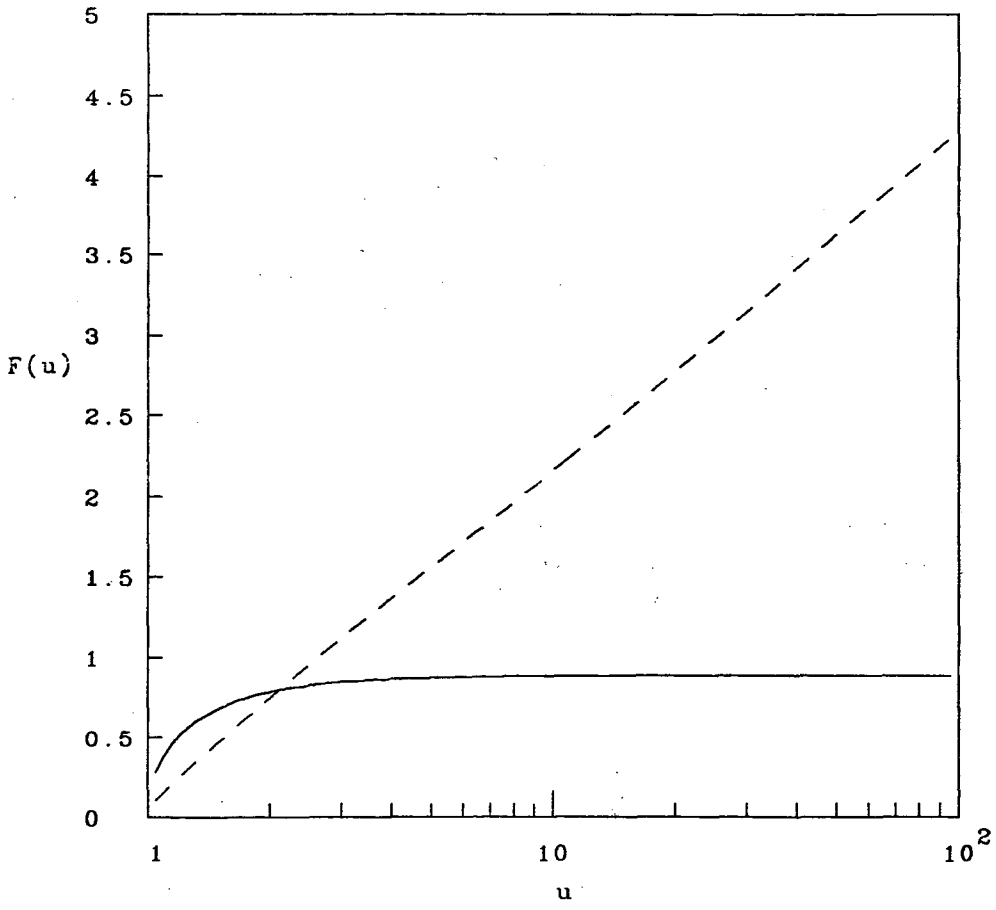

Fig. 15. The heavy quark production cross section function, $F_{q\bar{q}}$ (solid) and F_{gg} (dashed) vs. u. See. Eqs.(99) - (102).

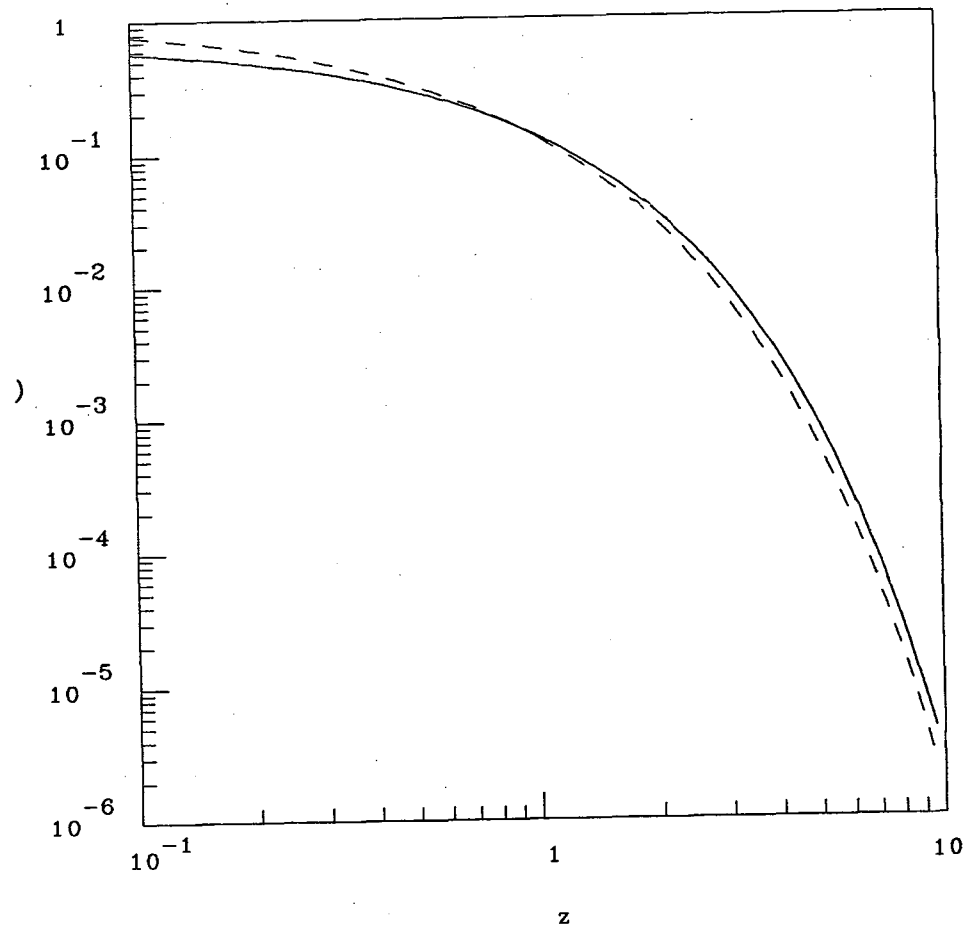

Fig. 16. The heavy quark production functions $G_{q\bar{q}}$ (solid) and G_{gg} (dashed) vs. z. See Eq. (109).

$s \to \infty$, $\sigma_{Q\overline{Q}}$ becomes a constant, dominated by the gg contribution. In Table VIII, we show predictions based on this simple model for c and b quarks with masses 1.5 GeV and 5 GeV and for hypothetical t-quarks with mass either 20 GeV or 40 GeV. We see that the predicted charm cross section is quite small, suggesting that these mechanisms are not the only ones contributing in the Fermilab and ISR range. Thus we regard these predictions as conservative estimates for the production of heavier quarks.

Table VIII. Heavy quark production in $p\overline{p}$ collisions through the mechanisms discussed in Section 2.7. See Eq.(110).

$\sqrt{s}$	$q\overline{q} \to Q\overline{Q}$	$gg \to Q\overline{Q}$
$c\overline{c}$:	$m = 1.5$GeV	
60GeV	$1 \cdot 10^{-30}$cm^2	$5 \cdot 10^{-30}$cm^2
540GeV	$3 \cdot 10^{-30}$cm^2	$40 \cdot 10^{-30}$cm^2
2000GeV	$4 \cdot 10^{-30}$cm^2	$50 \cdot 10^{-30}$cm^2
$b\overline{b}$:	$m = 5$GeV	
60GeV	$1.5 \cdot 10^{-32}$cm^2	$6 \cdot 10^{-33}$cm^2
540GeV	$2 \cdot 10^{-31}$cm^2	$2 \cdot 10^{-30}$cm^2
2000GeV	$3 \cdot 10^{-31}$cm^2	$3 \cdot 10^{-30}$cm^2
$t\overline{t}$:	$m = 20$GeV	
540GeV	$4 \cdot 10^{-33}$cm^2	$1 \cdot 10^{-32}$cm^2
2000GeV	$1 \cdot 10^{-32}$cm^2	$1 \cdot 10^{-31}$cm^2
$t\overline{t}$:	$m = 40$GeV	
540GeV	$3 \cdot 10^{-34}$cm^2	$2 \cdot 10^{-34}$cm^2
2000GeV	$2 \cdot 10^{-33}$cm^2	$1 \cdot 10^{-32}$cm^2

Appendix

Here we summarize the major points of the SU(2) x U(1) theory of electroweak interactions which are needed for deriving the fundamental properties of the W and Z bosons. The SU(2) x U(1) theory is a generalization of the usual theory of electromagnetism in which the coupling of fermions to the photon,

$$\overline{\psi}\, eQ\, A_\lambda \gamma^\lambda\, \psi, \tag{A1}$$

(where Q measures the charge of the fermion destroyed by ψ in units of e) is replaced by

$$\overline{\psi}[g\mathbf{T}\cdot\mathbf{W}_\lambda + g'\frac{Y}{2}B_\lambda]\gamma^\lambda\, \psi, \tag{A2}$$

where **T** represents weak isospin and contains implicitly a factor $(1-\gamma_5)/2$ to project out the left-handed piece of the fermion. The weak hypercharge is represented by Y which is related to the usual electric charge by

$$Q = T_3 + \frac{1}{2}Y. \tag{A3}$$

Assigning all left-handed fermions to doublets of weak isospin, and right-handed fermions to singlets, we derive the following table:

	e_L^-	e_R^-	ν_L	u_L	u_R	d_L	d_R
Q	-1	-1	0	2/3	2/3	$-1/3$	$-1/3$
T_3	$-1/2$	0	1/2	1/2	0	$-1/2$	0
Y	-1	-2	-1	1/3	4/3	1/3	$-2/3$

If we define

$$W^\pm = \frac{1}{\sqrt{2}}(W_1 \pm iW_2),\ T^\pm = T_1 \pm iT_2, \tag{A4}$$

we have the couplings

$$\overline{\psi}\left[g(T_3W_3 + \frac{1}{\sqrt{2}}T^+W_\lambda^- + \frac{1}{\sqrt{2}}T^-W_\lambda^+) + g'\frac{Y}{2}B_\lambda\right]\gamma^\lambda\psi. \tag{A5}$$

The charged W couplings produce the usual charged current interactions. Consider, for example, $\mu^- \to e^-\,\overline{\nu}_e\,\nu_\mu$. The usual V-A theory interaction is

$$\frac{G_F}{\sqrt{2}}\overline{\nu}_\mu\gamma^\lambda(1-\gamma_5)\mu\,\overline{e}\,\gamma_\lambda(1-\gamma_5)\nu_e \tag{A6}$$

On the other hand, putting in $1/M_W^2$ for the W propagator, our model gives

$$\left(\frac{g}{\sqrt{2}}\right)^2 \overline{\nu}_\mu \gamma^\lambda \frac{1}{2}(1-\gamma_5)\mu \frac{1}{M_W^2} \overline{e}\gamma_\lambda \frac{1}{2}(1-\gamma_5)\nu_e, \tag{A7}$$

so we can make the indentification

$$\frac{G_F}{\sqrt{2}} = \frac{g^2}{8M_W^2}. \tag{A8}$$

The gauge vector fields W and B are also coupled to scalars according to

$$\left|(g\mathbf{W}_\mu \cdot \mathbf{T} + g' B_\mu \frac{1}{2} Y)\phi\right|^2. \tag{A9}$$

Here ϕ is a multiplet with T=1/2 and Y=1:

$$\phi = \begin{pmatrix} \phi^+ \\ \phi^0 \end{pmatrix}, \tag{A10}$$

and the electrically neutral part has a vacuum expectation value:

$$<\phi> = \begin{pmatrix} 0 \\ v \end{pmatrix}. \tag{A11}$$

Thus

$$\left(g\mathbf{W}\cdot\mathbf{T} + g'\frac{1}{2}YB\right) <\phi> = \begin{pmatrix} \frac{g}{\sqrt{2}} W^- v \\ -\frac{1}{2} g W_3 v + \frac{1}{2} g' B v \end{pmatrix}. \tag{A12}$$

The scalar interaction, Eq. (A9), through this vacuum expectation value, produces masses for some of the vector bosons:

$$\frac{g^2}{2} W^- W^+ v^2 + \frac{1}{4}(gW_3 - g'B)^2 v^2. \tag{A13}$$

This term gives equal masses to the W^+ and W^-:

$$M_W^2 = \frac{g^2 v^2}{4}. \tag{A14}$$

The massive neutral vector field with proper normalization is seen from Eq.(A13) to be

$$Z = \frac{gW_3 - g'B}{\sqrt{g^2 + g'^2}}. \tag{A15}$$

Thus the Z mass is given by

$$M_Z^2 = \frac{g^2 + g'^2}{4} v^2. \tag{A16}$$

The orthogonal linear combination of neutral fields is massless:

$$A = \frac{g'W_3 + gB}{\sqrt{g^2 + g'^2}}. \tag{A17}$$

Defining $\tan\theta = g'/g$, we have

$$\begin{aligned} A &= \sin\theta\, W_3 + \cos\theta\, B \quad ; \quad W_3 = \sin\theta\, A + \cos\theta\, Z \\ Z &= \cos\theta\, W_3 - \sin\theta\, B \quad ; \quad B = \cos\theta\, A - \sin\theta\, Z \end{aligned} \tag{A18}$$

and the relation between the W and Z masses

$$M_Z^2 = M_W^2/\cos^2\theta. \qquad (A19)$$

Now we can express the original gauge interaction in terms of the physical fields W^+, W^-, Z, and A . The term in square brackets in Eq.(A5) becomes

$$\frac{g}{\sqrt{2}}(T^+W^- + T^-W^+) + g\sin\theta QA + \frac{g}{\cos\theta}(T_3 - \sin^2\theta Q)Z. \qquad (A20)$$

Thus we conclude

$$e = g\sin\theta\,, \qquad (A21)$$

which we can summarize with the mnemonic

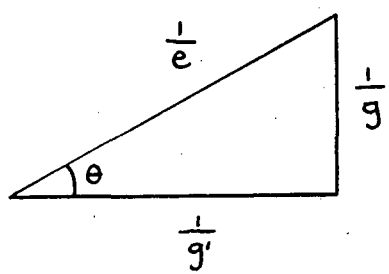

Using the measured value for $\sin^2\theta = 0.21$, we can find the W mass:

$$M_W^2 = \frac{\sqrt{2}g^2}{8G_F} = \frac{\pi\alpha}{\sqrt{2}\sin^2\theta G_F} = (81\,\mathrm{GeV})^2. \qquad (A22)$$

We can calculate the partial widths of the Z and W. The W^+ decays into $e^+\,\nu_e$ with a matrix element (ϵ is the W polarization vector)

$$\mathcal{M} = \frac{g}{\sqrt{2}}\epsilon_\lambda \overline{\nu}_e\gamma^\lambda\frac{1}{2}(1-\gamma_5)e. \qquad (A23)$$

Quite generally, a vector of mass M decaying into two light fermions with a matrix element

$$\mathcal{M} = \frac{1}{2}\epsilon_\lambda \overline{f}\gamma^\lambda(g_V + g_A\gamma_5)f', \qquad (A24)$$

has a width

$$\Gamma = \frac{1}{48\pi}(g_V^2 + g_A^2)M. \qquad (A25)$$

Thus we find the partial width

$$\Gamma(W\to e\nu) = \frac{\alpha M_W}{12\sin^2\theta} = 240\mathrm{MeV}. \qquad (A26)$$

For the full width of the W, we add three times this for the $u\overline{d}$ (to account for color) and multiply by three for the number of fermion generations, to obtain a full width

$$\Gamma(W) = \frac{\alpha M_W}{\sin^2\theta} = 2.8\,\mathrm{GeV}. \qquad (A27)$$

For the Z, the appropriate couplings to a given fermion pair are, from Eq.(A20)

$$g_V = \frac{e}{\sin\theta\cos\theta}(T_3 - 2Q\sin^2\theta),$$
$$g_A = \frac{e}{\sin\theta\cos\theta}(-T_3). \qquad (A28)$$

Thus the partial width to $\nu_e\overline{\nu}_e$ is

$$\Gamma(Z \to \nu_e\overline{\nu}_e) = \frac{\alpha M_Z}{24\sin^2\theta\cos^2\theta} = 170\text{MeV}. \qquad (A29)$$

The partial widths to ν, e, u, and d are in the proportions

$$\begin{aligned} 1 : 1 - 4\sin^2\theta + 8\sin^4\theta &: 3(1 - \frac{8}{3}\sin^2\theta + \frac{32}{9}\sin^4\theta) \\ &: 3(1 - \frac{4}{3}\sin^2\theta + \frac{8}{9}\sin^4\theta) \\ \approx 1 : 0.5 : 1.8 &: 2.3 \end{aligned} \qquad (A30)$$

Including a factor three for the number of generations, we find the branching ratio into e^+e^-

$$\begin{aligned} B(Z \to e^+e^-) &= \frac{1 - 4\sin^2\theta + 8\sin^4\theta}{24(1 - 2\sin^2\theta + \frac{8}{3}\sin^4\theta)} \\ &\approx 0.031 \end{aligned} \qquad (A31)$$

and the total width of the Z

$$\begin{aligned} \Gamma(Z) &= \frac{\alpha M_Z}{\sin^2\theta\cos^2\theta}(1 - 2\sin^2\theta + \frac{8}{3}\sin^4\theta) \\ &\approx 2.8\,\text{GeV} \end{aligned} \qquad (A32)$$

If the Z and W widths are equal, then $\sin^2\theta = 0.2196$.

Footnotes

1. For a two-body to two-body scattering process with initial momenta p_a and p_b and final momenta p_c and p_d, the standard Mandelstam variables are $s = (p_a + p_b)^2$, $t = (p_a - p_c)^2$, and $u = (p_a - p_d)^2$.
2. Really, we should have $p_{cm}\sqrt{s}$ in place of s. The difference is of order m_p^2/s.
3. The erudite and/or older reader may wonder why there is no f-trajectory, that is, an even amplitude with $s^{1/2}$ behavior. Its effect is simulated by the $\log^2 s/s_0$ piece when $s < s_0$. We found we could do without any additional even terms, so they were omitted.

References

1. Abramowitz, M. and I. A. Stegun, eds., 1964, *Handbook of Mathematical Functions* , National Bureau of Standards.
2. Amaldi, U., and K. R. Schubert, 1980, *Nucl. Phys.* **B166**, 301.
3. Auberson, F., T. Kinoshita, and A. Martin, 1971 , *Phys. Rev.* **D3**, 3185.
4. Bethe, H. A., 1958 , *Ann. Phys.* **3**, 190.
5. Bjorken, J. D., 1979, in *Proceedings of Summer Institute on Particle Physics, Quantum Chromodynamics.*
6. Block, M. M., and R. N. Cahn, 1982a, to be published in *Phys. Letters B.*
7. Block, M. M., and R. N. Cahn, 1982b, to be published in *Phys. Letters B.*
8. Bodwin, G. T. and S. J. Brodsky, 1981, *Phys. Rev. Lett.* **47**, 1799.
9. Bourrely, C. and J. Fischer, 1973, *Nucl. Phys.* **B61**, 513.
10. Cahn, R. N.,1982a, in *Proceedings of the 17th Rencontre de Moriond on Elementary Particle Physics.*
11. Cahn, R. N., 1982b, *Zeit. Phys.* **C15**, 253.
12. Chew, G. F., 1966, *The Analytic S-Matrix* , W. A. Benjamin, New York.
13. Collins, J. C. and D. E. Soper, 1982, *Phys. Letters* **109B**, 388.

14. Combridge, B. L., J. Kripfganz, and J. Ranft, 1977, *Phys. Lett.* **70B**, 234.
15. Combridge, B. L., 1979, *Nucl. Phys.* **B151**, 429.
16. Cutler, R., and D. Sivers, 1978, *Phys. Rev.* **D17**, 196.
17. Duke, D. and C. Quigg, 1982, unpublished Fermilab note.
18. Eden, R. J., 1966, *Phys. Rev. Lett.* **16**, 39.
19. Eden, R. J., 1967, *High Energy Collisions of Elementary Particles* , Cambridge Univ. Press, 1967.
20. Erdély, A., 1953, *Higher Transcendental Functions, v. II* , McGraw-Hill, p.58.
21. Feynman, R. P., R. D. Field, and G. C. Fox, 1978, *Phys. Rev.* **D18**, 3320.
22. Fischer, J., 1981, *Physics Reports* **76**, 157.
23. Fischer, J. *et al.*, 1978, *Phys. Rev.* **D18**, 4271.
24. Froissart, M., 1961, *Phys. Rev.* **123**, 1053.
25. Giacomelli, G. and M. Jacob, 1979, *Physics Reports* **55**, 1.
26. Horgan, R., and M. Jacob, 1981, in the *Proceedings of the International School of Elementary Particle Physics, Kupari-Dubrovnik, 1981,* to be published.
27. Jackson, J. D.,1973, in the *Proceedings of the Fourteenth Scottish Universities Summer School in Physics, 1973,* R. L. Crawford and R. Jennings, eds., Academic Press, London, 1974.
28. Kang, K., and B. Nicolescu, 1975, *Phys. Rev.* **D11**, 2461.
29. Louvain-Northwestern Collaboration, private communication from

M. M. Block, 1982.

30. Łukaszuk, L. and B. Nicolescu, 1973, *Nuovo Cim. Lett.* **8**, 405.

31. Kinoshita, T.,1966, in *Perspectives in Modern Physics,* R. E. Marshak Ed., Wiley and Sons, New York, 1966, p.211

32. Martin, A.,1965, *Nuovo Cimento* **39**, 704.

33. Martin, A. and F. Cheung, 1970, *Analytic Properties and Bounds of the Scattering Amplitudes* , Gordon and Breach.

34. Martin, A.,1982a, *Zeit. Phys.* **C15**, 185.

35. Martin, A., 1982b. Private communication.

36. Owens, J. F., E. Reya, and M. Glück, 1978, *Phys. Rev.* **D18**, 1501.

37. I. Ya. Pomeranchuk, 1958, *Soviet Physics JETP* **7**, 499.

38. Schiff, L. I., 1968, *Quantum Mechanics* , Third Edition, McGraw-Hill, 1968.

39. Titchmarsh, E. C., 1939, *The Theory of Functions* , Oxford University Press, p. 176.

40. UA4 Collaboration, 1982a, *Phys. Letters* **115B**, 333.

41. UA4 Collaboration, 1982b, *Phys. Letters* **117B**, 126.

42. West, G. B., and D. Yennie, 1968 , *Phys. Rev* **172**, 1413.

This report was done with support from the Department of Energy. Any conclusions or opinions expressed in this report represent solely those of the author(s) and not necessarily those of The Regents of the University of California, the Lawrence Berkeley Laboratory or the Department of Energy.

Reference to a company or product name does not imply approval or recommendation of the product by the University of California or the U.S. Department of Energy to the exclusion of others that may be suitable.

TECHNICAL INFORMATION DEPARTMENT
LAWRENCE BERKELEY LABORATORY
UNIVERSITY OF CALIFORNIA
BERKELEY, CALIFORNIA 94720